Electromagnetic simulation of generators

Erol Kurt*, *Member, IEEE and TUBAV*
Department of Electrical & Electronics Engineering, Faculty of Technology, Gazi University, 06500 Teknikokullar , Ankara, Turkey

***ekurt@gazi.edu.tr**

Funded by the Erasmus+ Programme of the European Union

TÜRKİYE CUMHURİYETİ AVRUPA BİRLİĞİ BAKANLIĞI
REPUBLIC OF TURKEY MINISTRY FOR EU AFFAIRS

TÜRKİYE ULUSAL AJANSI
TURKISH NATIONAL AGENCY

ERASMUS + Project Code: 2015-1-TR01-KA203-021342
Innovative European Studies on Renewable Energy Systems
Ankara Meeting, 04-08 April 2016

Universidad del País Vasco
Euskal Herriko Unibertsitatea
The University of the Basque Country

KLAIPĖDOS UNIVERSITETAS

CONTENTS

- INTRODUCTION
- FINITE ELEMENT METHOD
- GENERTORS
- GENERATORS with MULTIPLE ROTORS/STATORS
- RESULTS

IESRES EU- ERASMUS+
ekurt@gazi.edu.tr

INTRODUCTION

- As a result of increasing trends on the wind energy applications, the explorations on different types of generators take attention world-widely.
- While many efforts have been given on modeling the new topologies of the electric machines, the cogging torque and phase voltage ripples have been main problems among the scientific manners.
- Since the multiple stator generators (MSGs) with permanent magnets (PMs) have higher energy densities compared to the other commercial generator systems, finite element analysis (FEA) of such generators shed a light on design optimization techniques on wind-related renewable energy explorations.

- PM generators with multiple stator systems can have minimal cogging torque values, if an appropriate design can be realized.
- In fact, the radially and angularly directed flux lines can help to minimize the undesired ripples and torques.
- According to the detailed analyses, the field morphology can have different orientations as also known from the claw pole machines, however the heating, loses and signal distortions become the main problems.
- In this lecture, main ideas on FEA in electromagnetics and its application to a novel axial flux generator will be given. At the end of the course a sufficient literature on the studied machines will be given.

FINITE ELEMENT ANALYSIS (FEA)

- Fundamental Concept of FEM
- Maxwell's equations
- Boundary value problems for potentials
- Nodal finite elements
- Edge finite elements

IESRES EU- ERASMUS+
ekurt@gazi.edu.tr

FUNDAMENTAL CONCEPT OF FEM

- A continuous field of a certain domain having infinite degrees of freedom is approximated by a set of piecewise continuous models with a number of finite regions called elements.

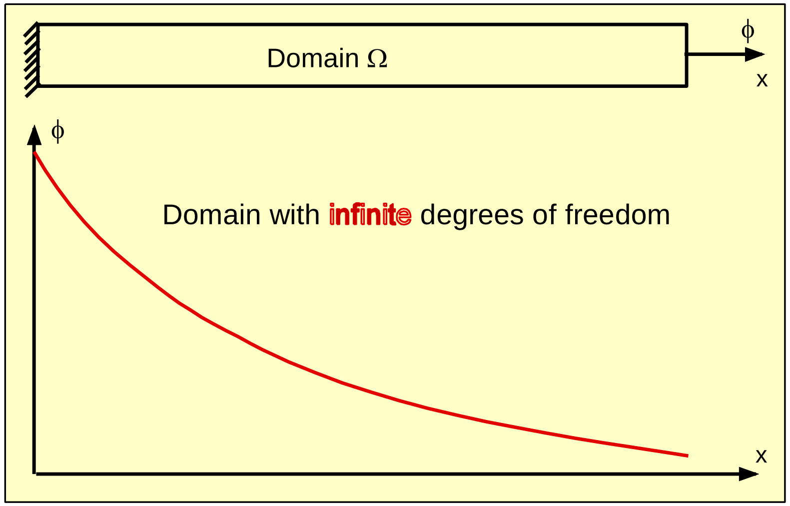

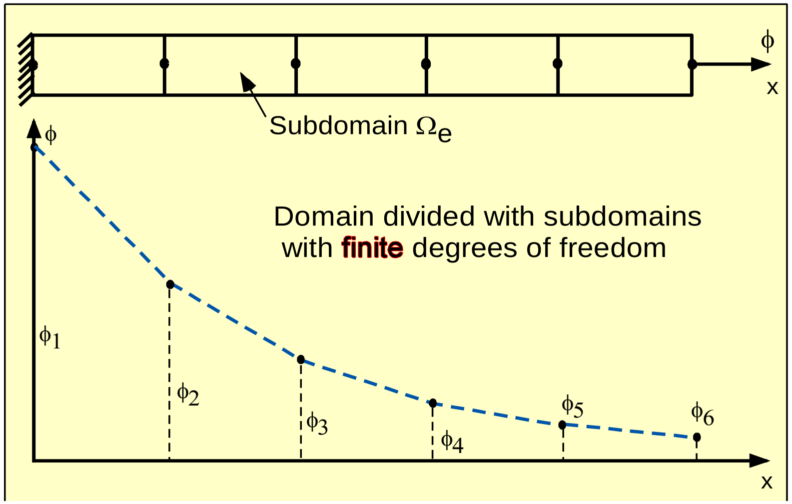

- Red line-Continuous field over the entire domain.
- Blue line-Finite number of linear approximations with the finite number of elements

IESRES EU- ERASMUS+
ekurt@gazi.edu.tr

Advantages of FEM are as follows:

- Model irregularly shaped bodies
- Compute general potential conditions
- Model bodies composed of different magnetic or non-magnetic materials (i.e. Ferromagnetic, diamagnetic and paramagnetic)
- Solve unlimited numbers and kinds of boundary conditions
- Able to use different element sizes in places where potential or general electromagnetic fields are concentrated
- Handle non-linear behavior using linear approximations
- Reduce System Cost

FEM Packages

FEM packages have 2 main types:

- Large Commercial Programs
  - Designed to solve many types of problems
  - Can be upgraded fairly easily
  - Initial Cost is high
  - Less efficient
- Special-purpose programs
  - Relatively short, low development costs
  - Additions can be made quickly
  - Efficient in solving their specific types of problems
  - Can't solve different types of problems

IESRES EU- ERASMUS+
ekurt@gazi.edu.tr

Some commercial packages are as follows:

- Algor
- ANSYS MAXWELL and FLUENT
- COSMOS/M
- STARDYNE
- IMAGES-3D
- MSC/NASTRAN
- SAP90
- GT-STRUDL
- SUPERFISH

IESRES EU- ERASMUS+
ekurt@gazi.edu.tr

FINITE ELEMENT METHOD

- Maxwell‘s equations

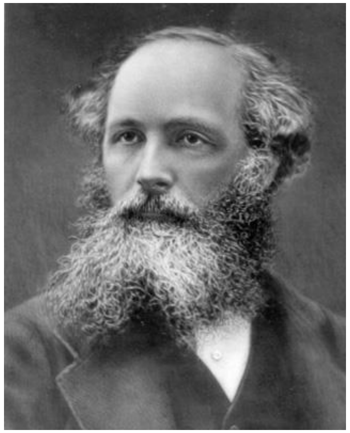

$$curl\mathbf{H} = \mathbf{J} + \frac{\partial \mathbf{D}}{\partial t}$$

$$curl\mathbf{E} = -\frac{\partial \mathbf{B}}{\partial t}$$

$$div\mathbf{B} = 0$$

$$div\mathbf{D} = \rho$$

$$\mathbf{B} = \mu\mathbf{H}; \quad \mathbf{J} = \sigma\mathbf{E}; \quad \mathbf{D} = \varepsilon\mathbf{E}$$

IESRES EU- ERASMUS+
ekurt@gazi.edu.tr

- A numerical solution method for a well-defined material and media
- It solves differential equations
- Boundary values are important
- Everything should be defined in a closed solution cell

In order to solve an electromagnetic problem, the fields on a certain computational volume should be determined. Therefore the main fields for that purpose are POTENTIALS (i.e. $\boldsymbol{A}$ and V). Thus for these potentials, one should determine the boundary values on the structure.

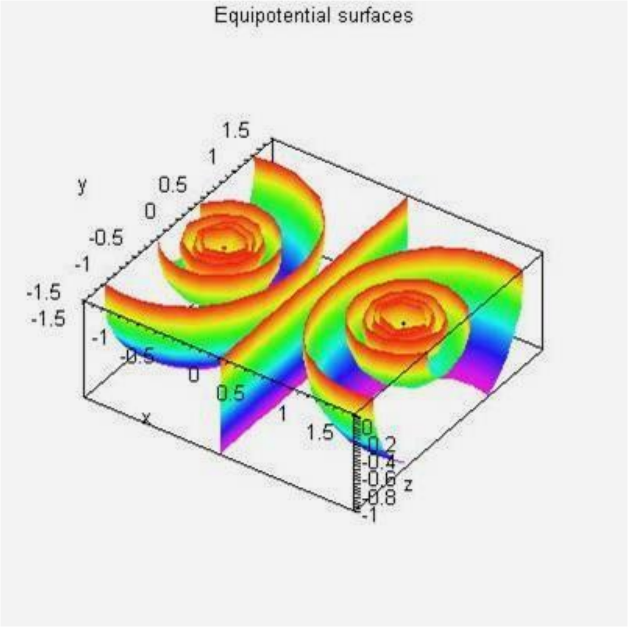

- Boundary value problems for potentials:
  - ✓ Continuous functions
  - ✓ Satisfy second order differential equations
  - ✓ Neumann and Dirichlet boundary conditions

- Boundary value problems for potentials

  - ✓ Continuous functions
  - ✓ Satisfy second order differential equations
  - ✓ Neumann and Dirichlet boundary conditions

IESRES EU- ERASMUS+
ekurt@gazi.edu.tr

- Boundary value problems for potentials

  - ✓ Continuous functions
  - ✓ Satisfy second order differential equations
  - ✓ Neumann and Dirichlet boundary conditions

$$\mathbf{B} = curl\,\mathbf{A}$$

$$\mathbf{E} = -\frac{\partial \mathbf{A}}{\partial t} - grad\,\frac{\partial V}{\partial t}$$

- Boundary value problems for potentials
  - ✓ Satisfy second order differential equations

$$curl\mathbf{H} - \mathbf{J} - \frac{\partial \mathbf{D}}{\partial t} = \mathbf{0}$$

$$curl(\mu\, curl\mathbf{A}) + \sigma \frac{\partial \mathbf{A}}{\partial t} + \sigma grad \frac{\partial V}{\partial t} + \varepsilon \frac{\partial^2 \mathbf{A}}{\partial t^2} + \varepsilon grad \frac{\partial^2 V}{\partial t^2} = \mathbf{0}$$

$$div(\mathbf{J} + \frac{\partial \mathbf{D}}{\partial t}) = 0$$

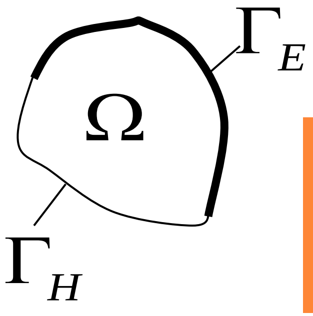

$$-div(\sigma \frac{\partial \mathbf{A}}{\partial t} + \sigma grad \frac{\partial V}{\partial t} + \varepsilon \frac{\partial^2 \mathbf{A}}{\partial t^2} + \varepsilon grad \frac{\partial^2 V}{\partial t^2}) = 0$$

in a closed domain Ω

- Boundary value problems for potentials
  - ✓ Neumann and Dirichlet boundary conditions

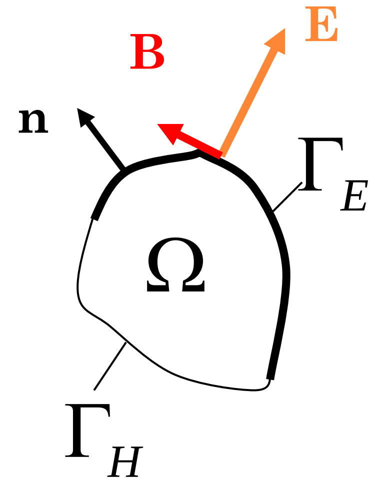

Prescription of tangential **E** (and normal **B**) on Γ_E:

$$\mathbf{E}\times\mathbf{n} = -\frac{\partial \mathbf{A}}{\partial t}\times\mathbf{n} - grad\,\frac{\partial V}{\partial t}\times\mathbf{n}$$

$$\mathbf{B}\cdot\mathbf{n} = \mathbf{n}\cdot curl\mathbf{A}$$

$$\mathbf{A}\times\mathbf{n} = \mathbf{a_0},$$

$$V = V_0$$

n is the outer unit normal at the boundary

- Boundary value problems for potentials
  - ✓ Neumann and Dirichlet boundary conditions

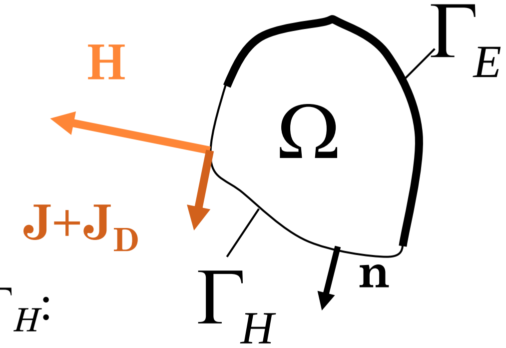

Prescription of tangential **H** (and normal **J+J$_\mathbf{D}$**) on Γ_H:

$$\mathbf{H}\times\mathbf{n} = \mu\, curl\mathbf{A}\times\mathbf{n},$$

$$(\mathbf{J}+\frac{\partial\mathbf{D}}{\partial t})\cdot\mathbf{n} = -\sigma(\frac{\partial\mathbf{A}}{\partial t} + grad\,\frac{\partial V}{\partial t})\cdot\mathbf{n} - \varepsilon(\frac{\partial^2\mathbf{A}}{\partial t^2} + grad\,\frac{\partial^2 V}{\partial t^2})\cdot\mathbf{n}$$

$$\mu\, curl\mathbf{A}\times\mathbf{n} = \mathbf{K},$$

$$\sigma(\frac{\partial\mathbf{A}}{\partial t} + grad\,\frac{\partial V}{\partial t})\cdot\mathbf{n} + \varepsilon(\frac{\partial\mathbf{A}^2}{\partial t^2} + grad\,\frac{\partial V^2}{\partial t^2})\cdot\mathbf{n} = -J$$

- **Finite element discretization**

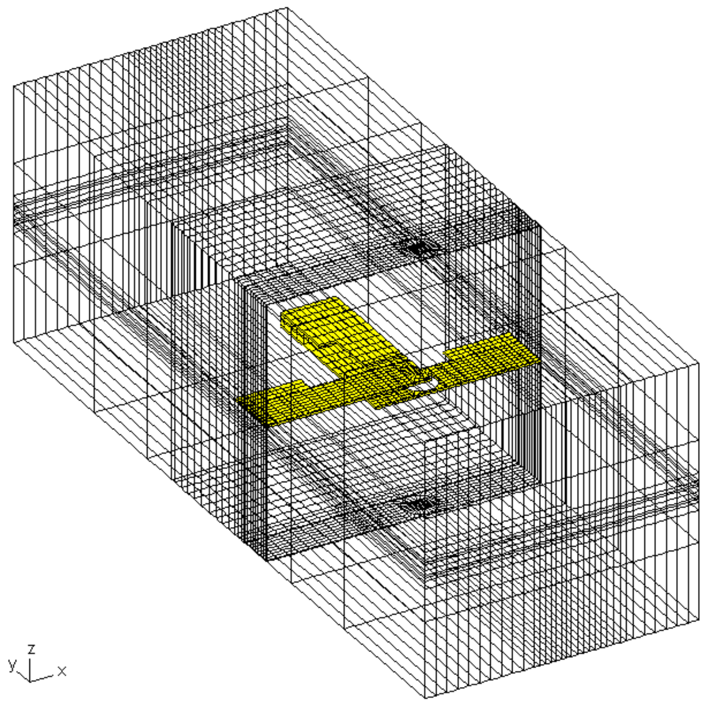

IESRES EU- ERASMUS+
ekurt@gazi.edu.tr

Nodal finite elements

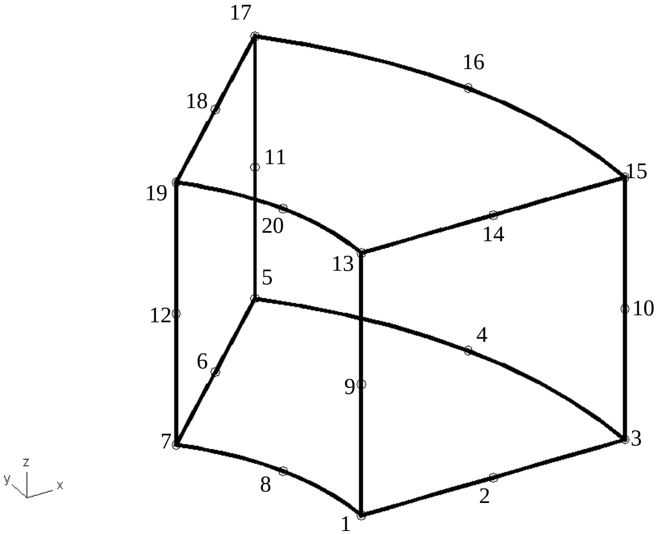

Shape functions:

$$N_i(\mathbf{r}) = \begin{cases} 1 \text{ in node } i, \\ 0 \text{ in all other nodes.} \end{cases}$$

$i = 1, 2, \ldots, n_n$

IESRES EU- ERASMUS+
ekurt@gazi.edu.tr

- **Nodal finite elements**

Corner node

Midside node

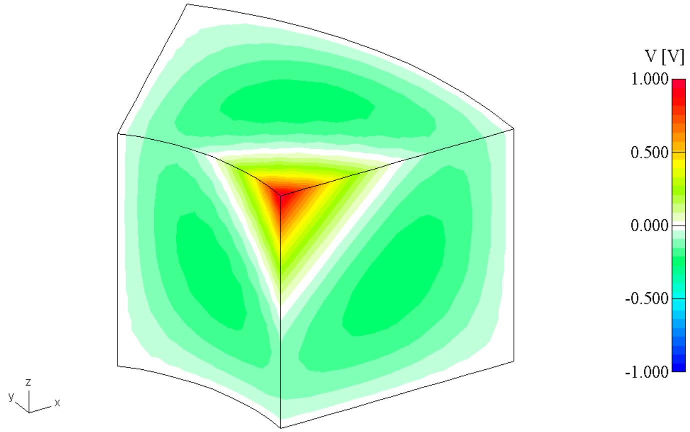

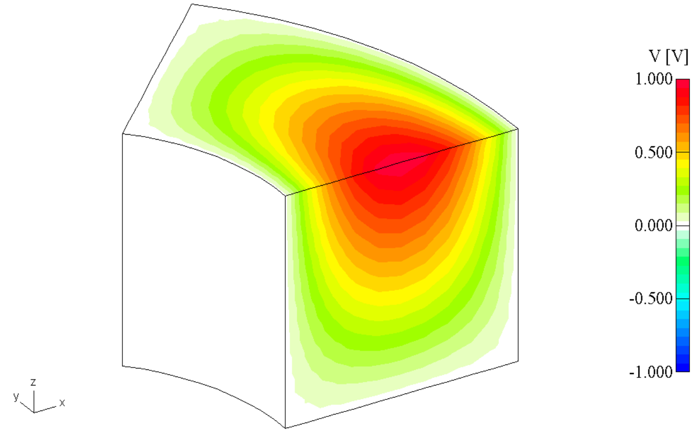

Shape functions:

$$N_i(\mathbf{r}) = \begin{cases} 1 \text{ in node } i, \\ 0 \text{ in all other nodes.} \end{cases}$$

$i = 1, 2, \ldots, n_n$

Nodal finite elements

Basis functions for scalar quantities (e.g. *V*):

Number of nodes: n_n, **number of nodes on** Γ_D: n_{Dn}

$$n = n_n - n_{Dn},$$

nodes on Γ_D: $n+1, n+2, \ldots, n_n$

$$V(\mathbf{r},t) \approx V^{(n)} = \sum_{k=1}^{n} V_k(t) N_k(\mathbf{r})$$

Linear independence of nodal shape functions

$$\sum_{i=1}^{n_n} N_i = 1$$

Taking the gradient:

$$\sum_{i=1}^{n_n} grad\, N_i = 0$$

The number of linearly independent gradients of the shape functions is n_n-1 (tree edges)

- Edge finite element

Edge basis functions:

$$\int_{Edge_j} \mathbf{N}_i(\mathbf{r}) \cdot d\mathbf{l} = \begin{cases} 1, & \text{if } \ i = j, \\ 0, & \text{if } \ i \neq j. \end{cases}$$

$\boldsymbol{i = 1, 2, \ldots, n_e}$

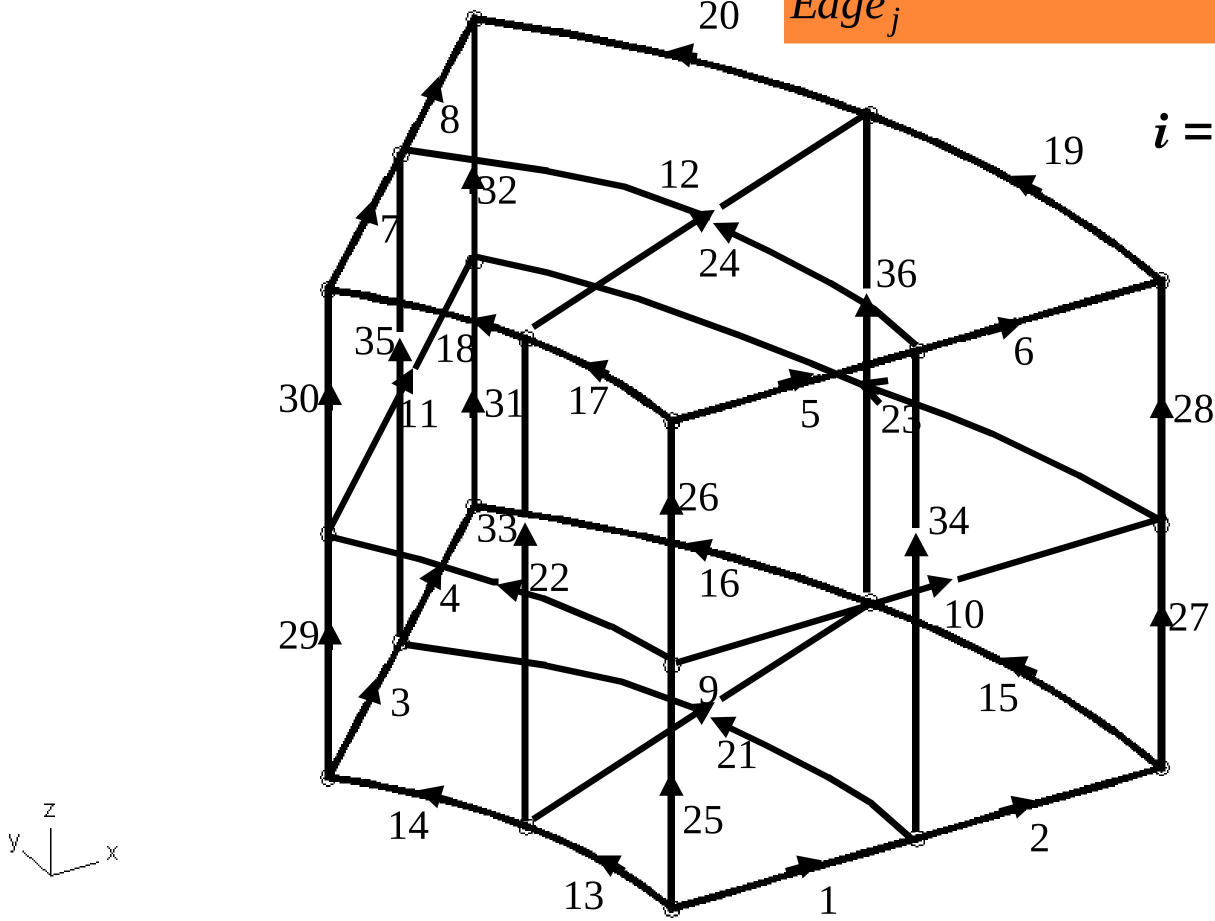

- Edge finite element

Basis functions

Side edge	**Across edge**

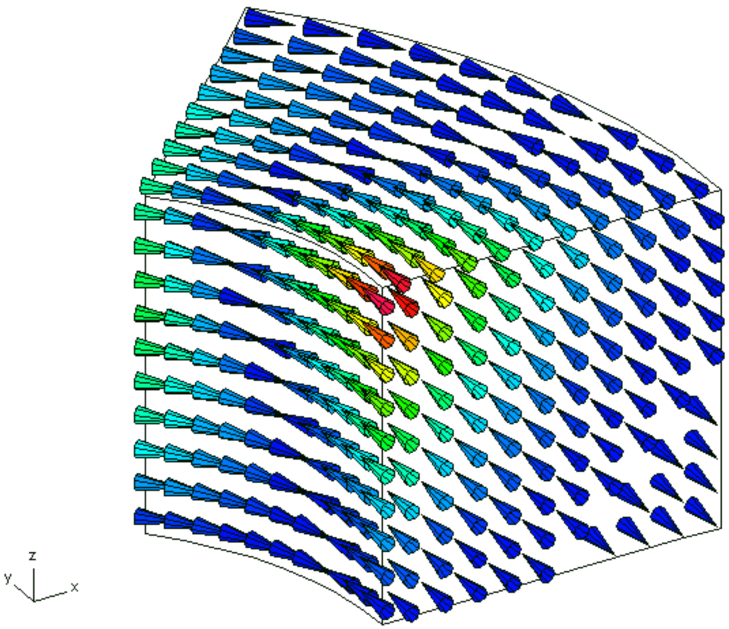

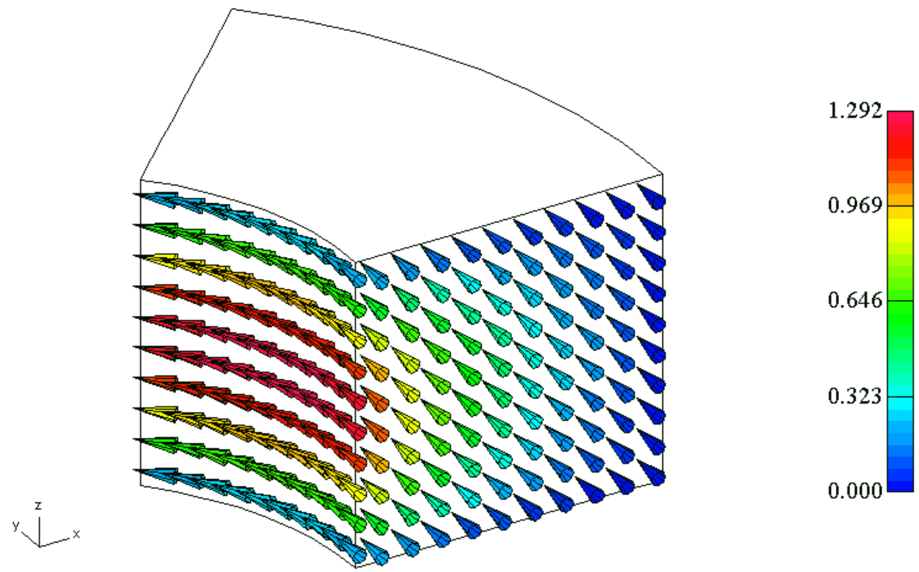

Edge finite element

Basis functions for vector intensities (e.g. A):

Number of edges: n_e, number of edges on Γ_D: n_{De}

$$n = n_e - n_{De},$$ **edges on Γ_D: $n+1$, $n+2$, ..., n_e**

$$\mathbf{A}(\mathbf{r},t) \approx \mathbf{A}^{(n)} = \sum_{k=1}^{n} a_k(t)\mathbf{N}_k(\mathbf{r})$$

IESRES EU- ERASMUS+
ekurt@gazi.edu.tr

FINITE ELEMENT METHOD …

- Samples

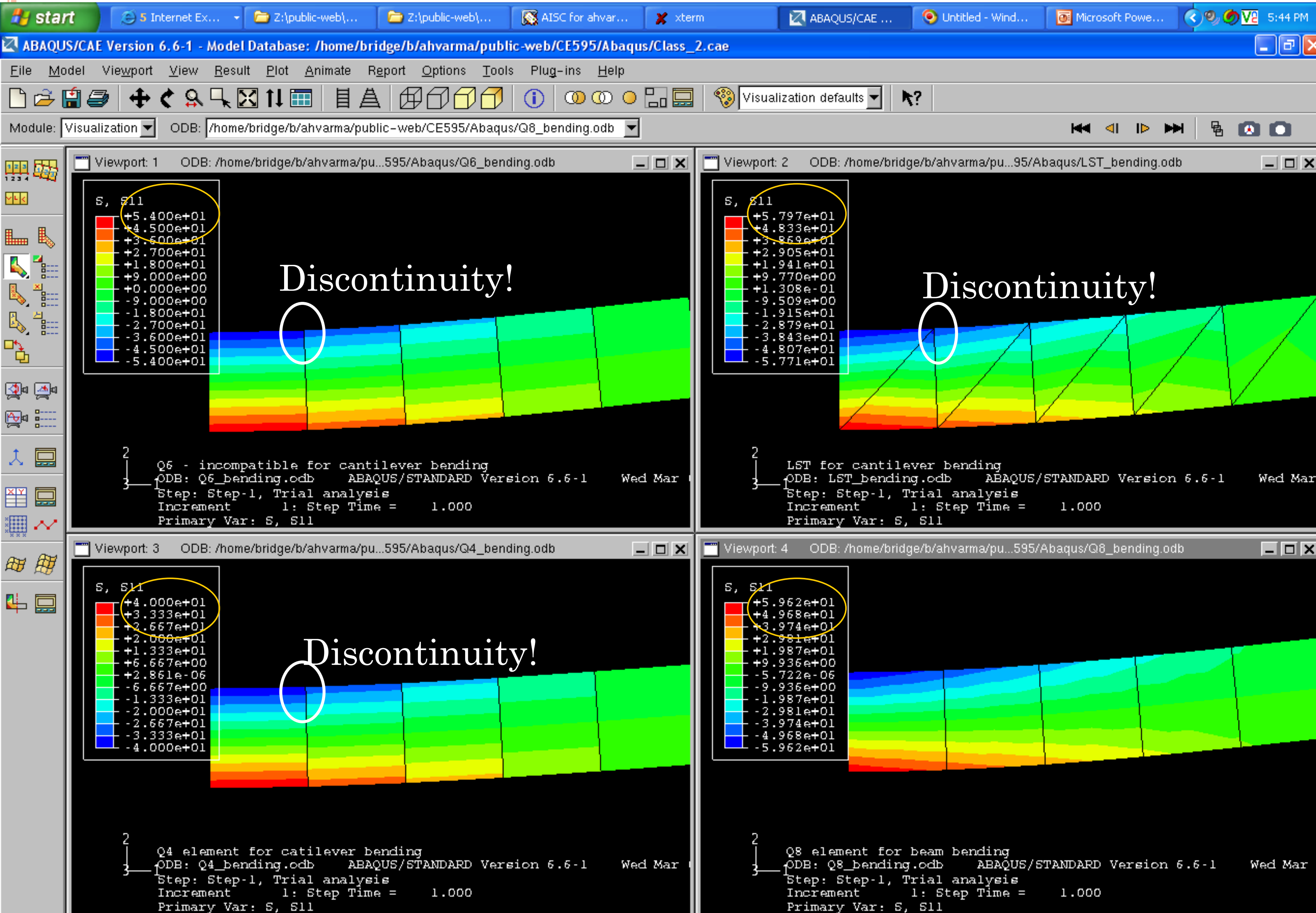

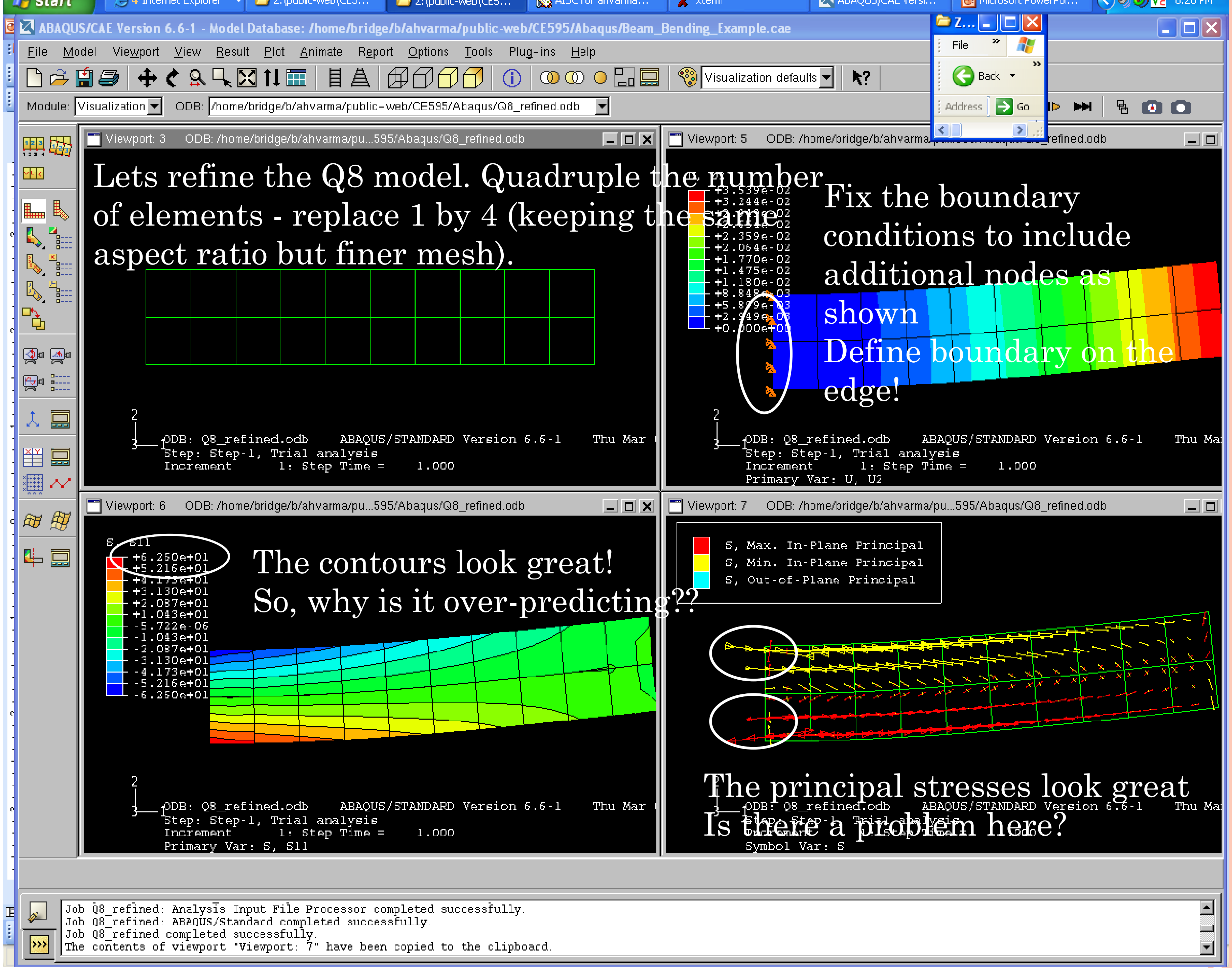
ABAQUS/CAE Version 6.6-1 - Model Database: /home/bridge/b/ahvarma/public-web/CE595/Abaqus/Beam_Bending_Example.cae
File Model Viewport View Result Plot Animate Report Options Tools Plug-ins Help
Visualization defaults
Module: Visualization
ODB: /home/bridge/b/ahvarma/public-web/CE595/Abaqus/Q8_refined.odb
Viewport: 3 ODB: /home/bridge/b/ahvarma/pu...595/Abaqus/Q8_refined.odb
Lets refine the Q8 model. Quadruple the number of elements - replace 1 by 4 (keeping the same aspect ratio but finer mesh).
ODB: Q8_refined.odb ABAQUS/STANDARD Version 6.6-1 Thu Mar
Step: Step-1, Trial analysis
Increment 1: Step Time = 1.000
Viewport: 5 ODB: /home/bridge/b/ahvarma
+3.244e-02
+2.359e-02
+2.064e-02
+1.770e-02
+1.475e-02
+1.180e-02
+0.000e+00
Fix the boundary conditions to include additional nodes as shown
Define boundary on the edge!
ODB: Q8_refined.odb ABAQUS/STANDARD Version 6.6-1 Thu Mar
Step: Step-1, Trial analysis
Increment 1: Step Time = 1.000
Primary Var: U, U2
Viewport: 6 ODB: /home/bridge/b/ahvarma/pu...595/Abaqus/Q8_refined.odb
S, S11
+6.260e+01
+5.216e+01
+3.130e+01
+2.087e+01
+1.043e+01
-5.722e-06
-1.043e+01
-2.087e+01
-3.130e+01
-4.173e+01
-5.216e+01
-6.260e+01
The contours look great!
So, why is it over-predicting??
ODB: Q8_refined.odb ABAQUS/STANDARD Version 6.6-1 Thu Mar
Step: Step-1, Trial analysis
Increment 1: Step Time = 1.000
Primary Var: S, S11
Viewport: 7 ODB: /home/bridge/b/ahvarma/pu...595/Abaqus/Q8_refined.odb
S, Max. In-Plane Principal
S, Min. In-Plane Principal
S, Out-of-Plane Principal
The principal stresses look great
Is there a problem here?
Symbol Var: S
Job Q8_refined: Analysis Input File Processor completed successfully.
Job Q8_refined: ABAQUS/Standard completed successfully.
Job Q8_refined completed successfully.
The contents of viewport "Viewport: 7" have been copied to the clipboard.

INTRODUCTION TO GENERATORS

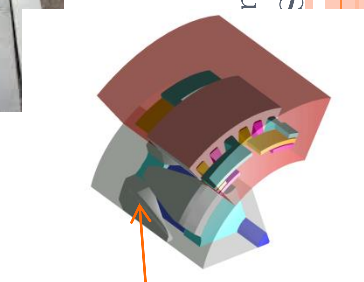

- GENERATORS
  - Axial flux
    - Single stator& rotor
    - Multiple stators& rotors
    - Double stators
    - Double rotors
    - Torus
    - Claw Pole
  - Radial flux

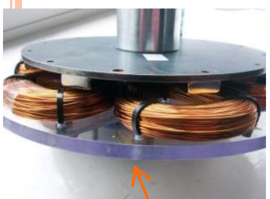

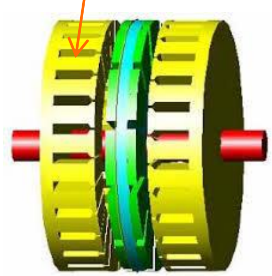

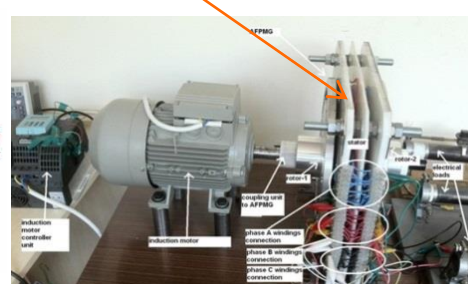

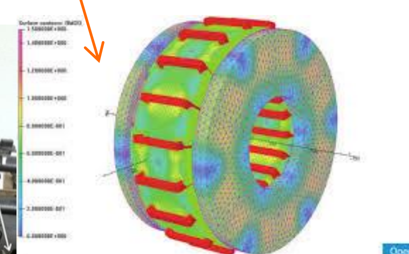

MOTIVATION

- The PMSGs suffer from the torque ripples arising from the electromagnetic design artifacts.
- The identification and the minimization of these ripples are of great importance in designing the machines.
- The parasitic torque ripples cause mechanical vibrations and acoustic noises in the machines.
- The most important contribution to the torque ripples is the cogging torque which stems from the magnetic interaction between the PMs and the stator slots.
- The air-gap reluctance should be constant as much as, when the rotor passes nearby the stator slots to minimize the torque ripples.
- There exist various cogging torque minimization techniques:

1. The slot/magnet skewing,
2. Displacing/shaping the magnets,
3. Employing dummy slots/teeth
4. Air-gap optimization techniques,

- In addition, second important artifact of the PMSGs is the temperature rise inside the machine.

Recent technological improvements on the production of permanent magnet (PM) materials and power electronics have enabled new design, construction and applications of permanent magnet synchronous generators (PMSGs).

The PMSGs are generally preferred over other generators and motors in the sense;

✓high efficiency,
✓high torque,
✓compact structure,
✓fast dynamic response.

If an appropriate air gap between rotor and stator and a suitable design shape are provided, one can use PMSGs in many applications which require minimal torque ripple, acoustic noise and reduced vibration.

CASE STUDY (2 TYPES OF GENERATORS)

- Here we introduce a new axial-flux permanent magnet generator in order to give as a case study.
- The machine has single stator and double rotors at the left- and right-hand sides.
- The generator has different magnetic flux lines depending on the positions of cores and magnets.
- It was designed for wind energy applications.
- The transient solutions of finite element analysis (FEA) are obtained based on the equivalent circuit models subjected to three groupings (i.e. phases) and output currents, voltages and cogging torque values are simulated at various speeds.
- The machine can have different power ranges as function of airgap. Here it gives 600 W with 8 mm airgap.

Numerical features and material constants

- Total number of mesh elements over the entire volume: 930612
- Permanent Magnets: XG196/96

(Magnetization= -763939A/m and density=7800kg/m^3)

- Cores: M19 (density=7650 kg/m^3)

Soft magnetic materials	Saturation flux density Bsat, [T] [1]	$H(\mu_{max})$, [A/m] [2]	Relative permeability μ, [-]	Electric conductivity γ, [MS]
M-19 Steel	1.99	79.577	4416	0

- Filling material: Polyester (electrical relative permitivity: 3.2)

SINGLE PHASE GENERATOR

The second generator has 12 cores and 24 coils in the stator and 24 magnets are located in two rotors. Gen 2 is a single phase generator, however it can be easily transformed to a 3 phase generator.

•The loaded tests prove that P=95W is available at ω=500 rpm.

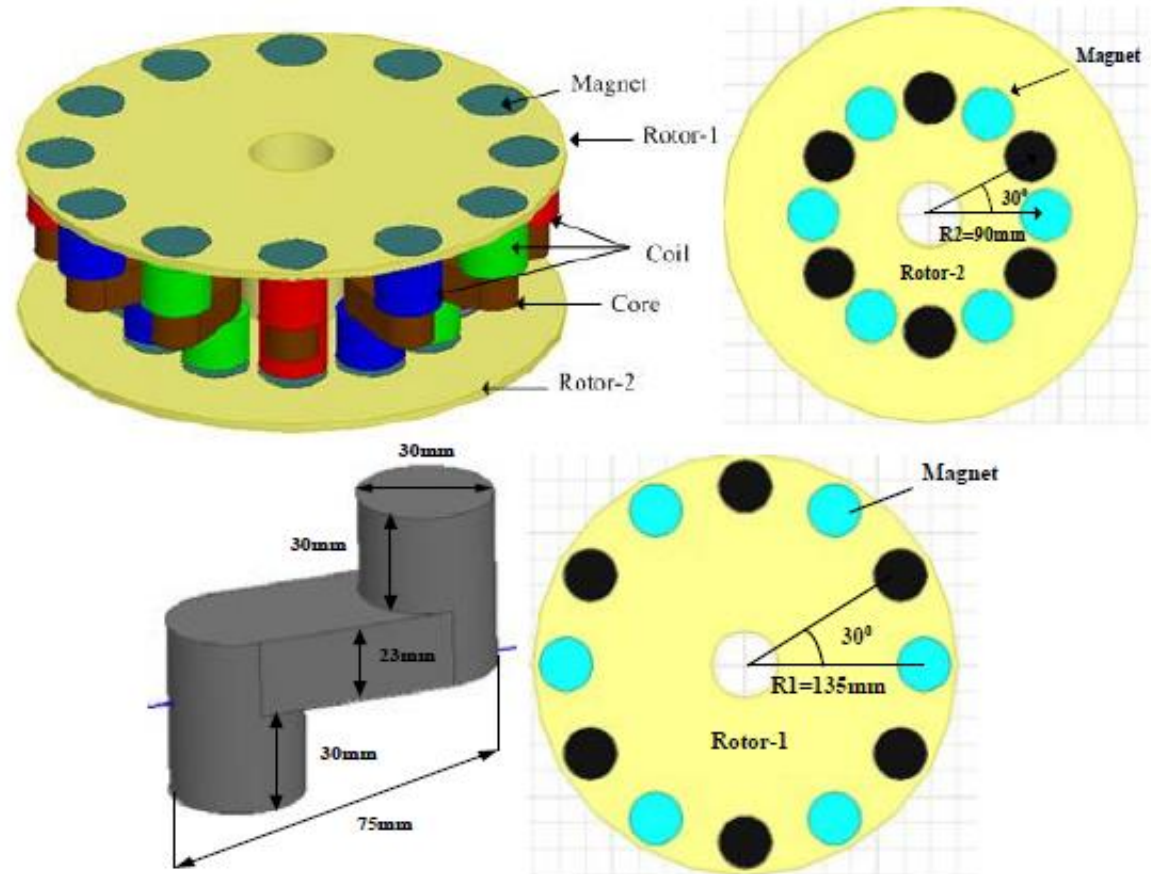

Fig. 3. Geometries of the second PMSG, two rotors with magnets and a core from the stator.

Theory of single phase structure

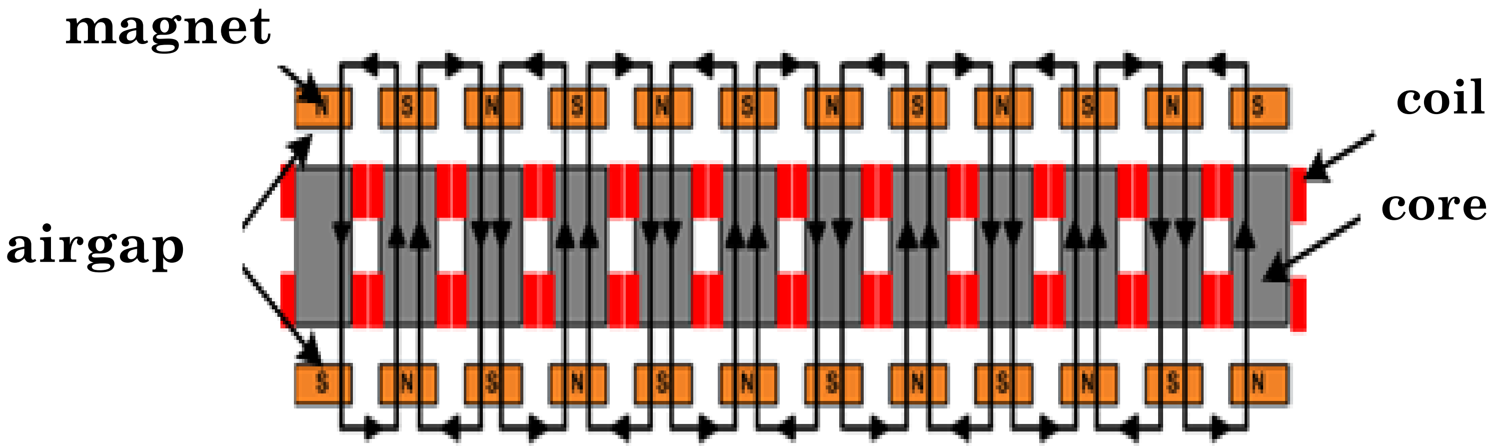

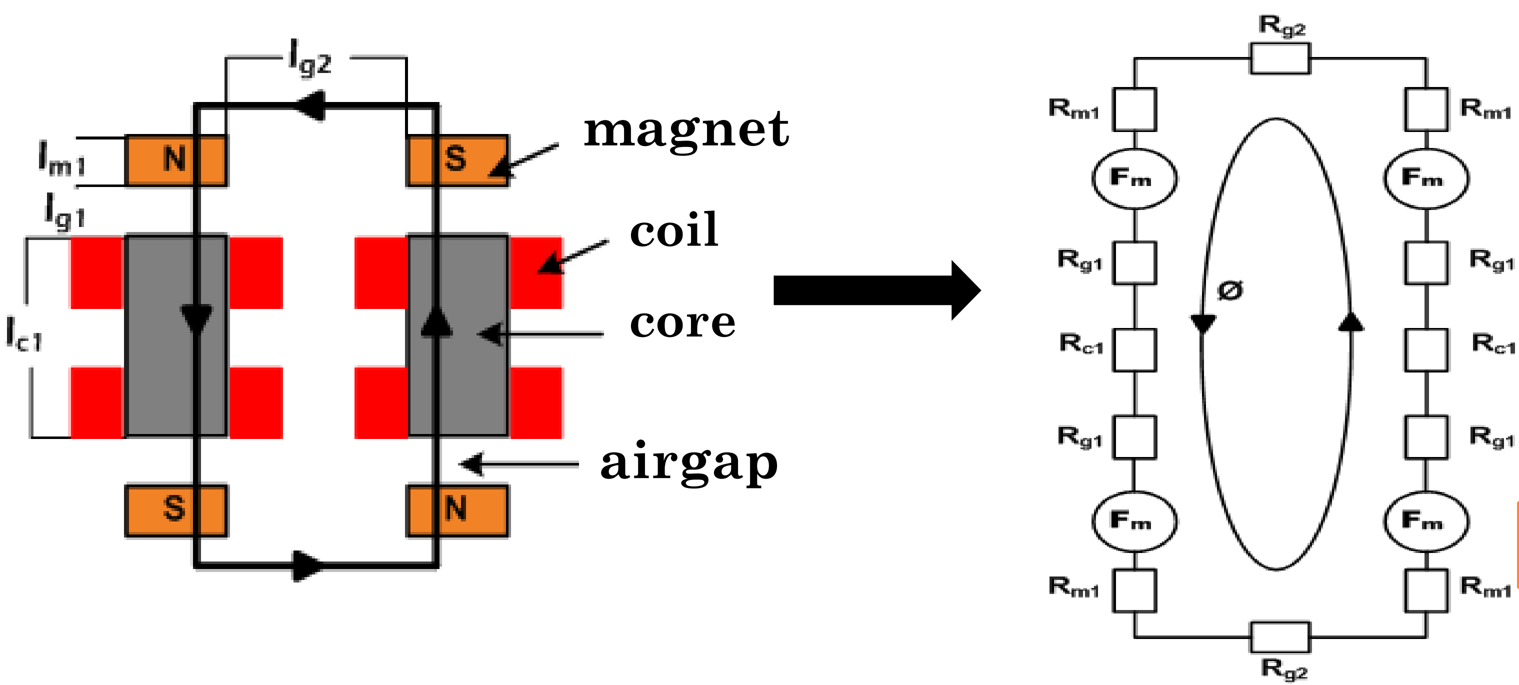

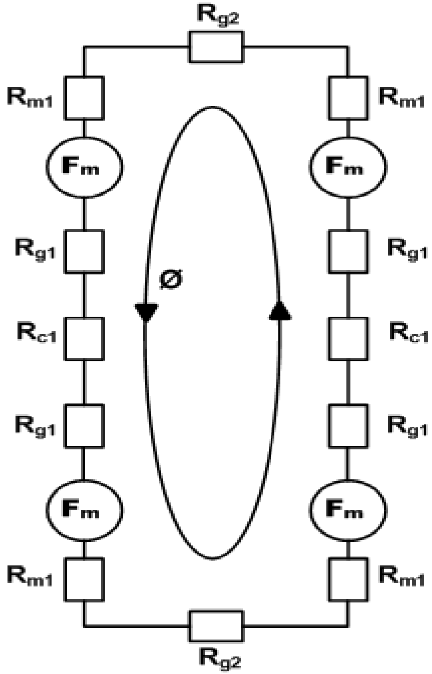

$l_g = 4.\, l_{g1} + 2.\, l_{g2}$ $\quad$ $l_m = 4.\, l_{m1}$ $\quad$ $l_c = 2.\, l_{c1}$

$$R_g = 4R_{g1} + 2R_{g2}$$

$$R_g = \frac{l_g}{\mu_o . A_g}$$

$$R_T = R_g + R_m + R_c$$

$$R_m = 4R_{m1}$$

$$R_m = \frac{l_m}{\mu_o . A_m}$$

$$R_c = 2R_{c1}$$

$$R_c = \frac{l_c}{\mu_{rc} . A_c}$$

R_g: Airgap reluctance
R_m Magnet reluctance
R_c: Core reluctance
R_T: Total reluctance

$$\phi = \frac{H_m . l_m}{R_T}$$

$$B_g = \frac{H_m . l_m}{R_T . A_g}$$

$$B_m = \mu_0 . \mu_{rm} . H_m + B_{rm}$$

$$B_g = \mu_0 . H_g$$

$$B_c = \mu_{rc} . H_c$$

B_m: Magnet flux density (T)
μ_0: Vacuum permeability (H/m)
μ_{rm} Magnet permeability (H/m)
H_m: Magnet magnetic field strenght (A/m)
B_{rm} Magnet reminiscence flux density (T)
B_c: Core flux density (T)

When the Ampere's Law is applied,

$$H_g.l_g + H_c.l_c = 4H_m.l_m$$

$$\emptyset = B_g.A_g = B_m.A_m = B_c.A_c$$

$$\emptyset(t) = \emptyset_{max}.\sin(wt)$$

$$\lambda = N_s.\phi$$

$$e = \frac{d\lambda}{dt}$$

$$e(t) = N_s\frac{d\phi}{dt}$$

$$e(t) = N_s.\phi_{max}.w.\cos(wt)$$

$$P = m.V_t.I.\cos\varphi$$

$$P = m.E.I$$

FLUX LINES

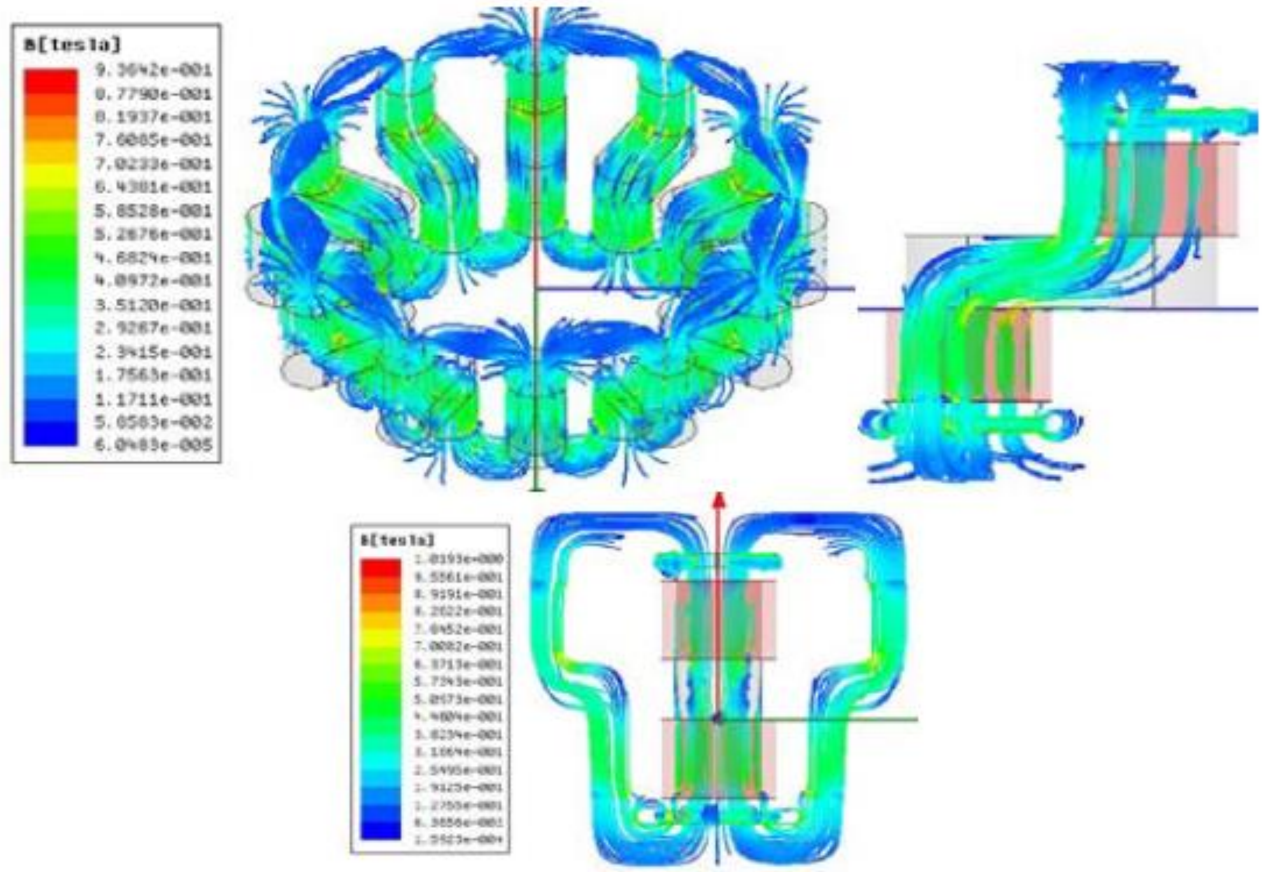

Fig. 5. Flux density lines.

Magnetodynamics simulations

- Magnetodynamics simulations have been performed for various angular velocities: ω=100-600 *rpm* are presented here.
- In order to generate a raw AC power with unregulated voltage, we assign each group with the sum of the parallel attached upper and lower coils. Within this circuitry, phase voltages for each branch of star configuration can be increased twofold.

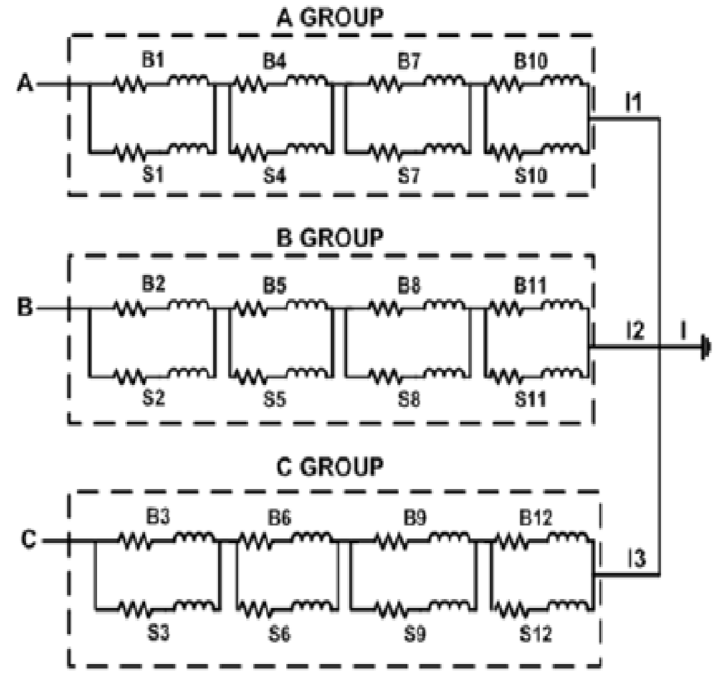

External circuit with three groupings *A*, *B* and *C*. Upper and lower coils are indicated by B_n and S_n.

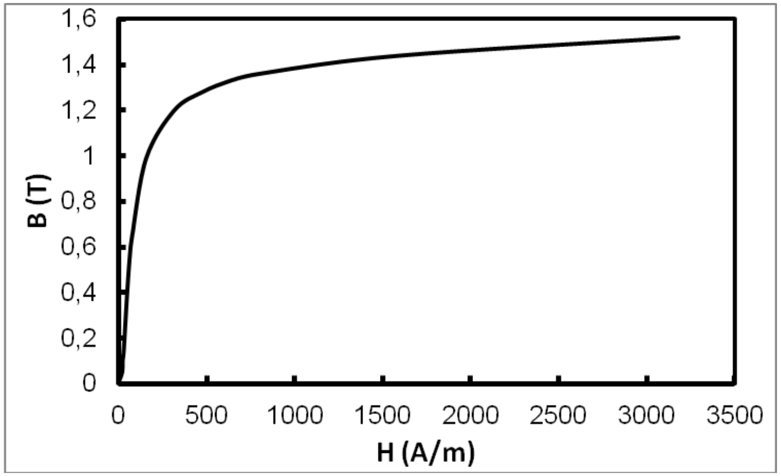

The B-H curve of core material in the simulation.

Design parameters of the proposed generator.

Components	Features
Inner radius of rotor R_2 (mm)	70
Outer radius of rotor R_2 (mm)	110
Inner radius of rotor R_1 (mm)	115
Outer radius of rotor R_1(mm)	155
Inner radius of stator disc (mm)	70
Outer radius of stator disc (mm)	155
Coil inner diameter (mm)	30
Coil outer diameter (mm)	40
Phase	1
Winding turns	200
Wire diameter (mm)	0.75
Magnet type	NdFeB
Magnet shape	circular
Magnet diameter (mm)	40
Magnet thickness (mm)	5
Core material	M19
Core type	axially laminated
Air gap (mm)	5
Core coefficients (W/m^3)	
K_h	164.2
K_c	1.3
K_e	1.72
K_{dc}	0

Magnetodynamics

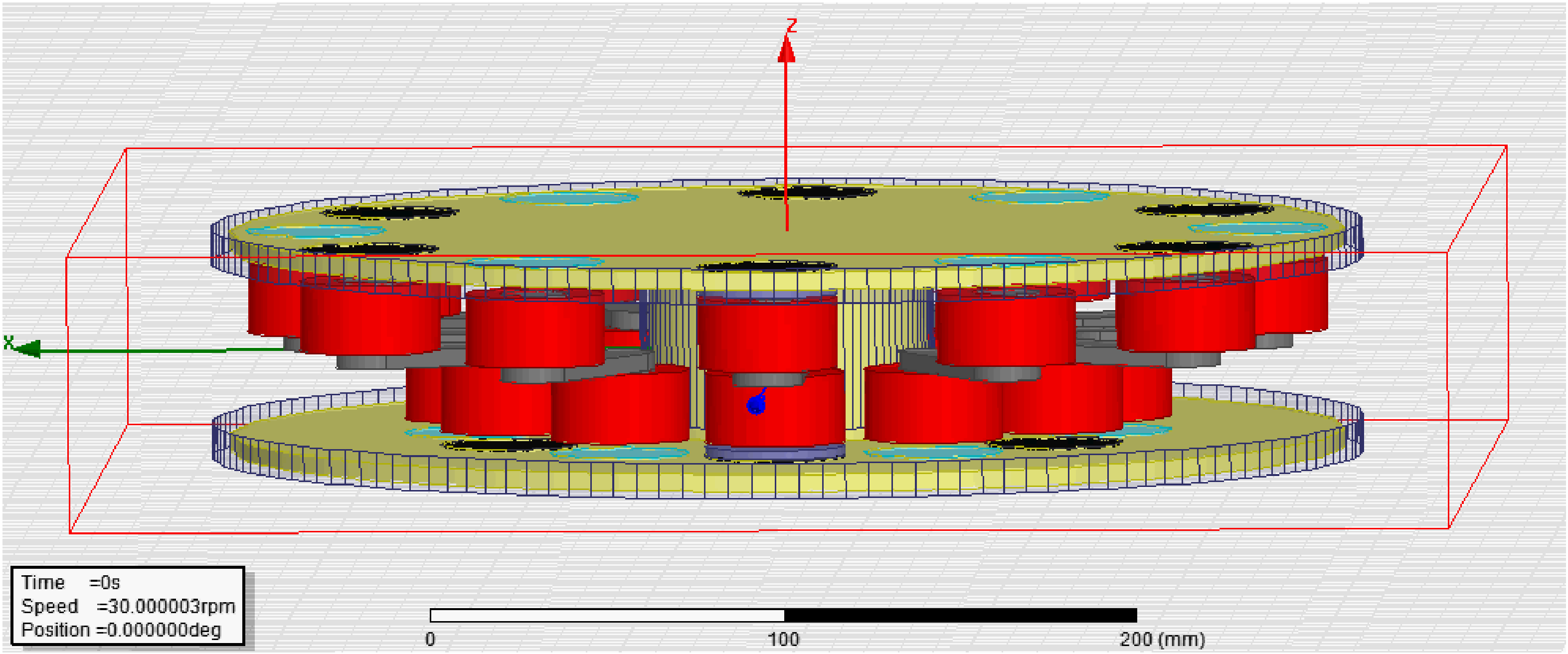

Results of simulation of Gen2

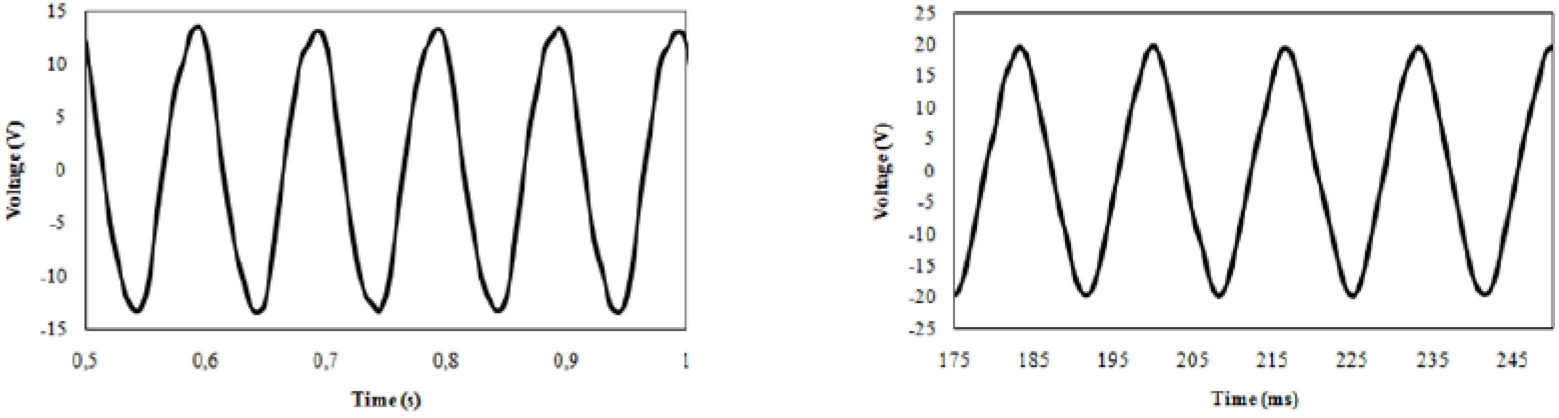

(a) b)

Fig. 9. Phase voltage versus time **a)** for ω=100 *rpm* and **b)** ω=600 *rpm*.

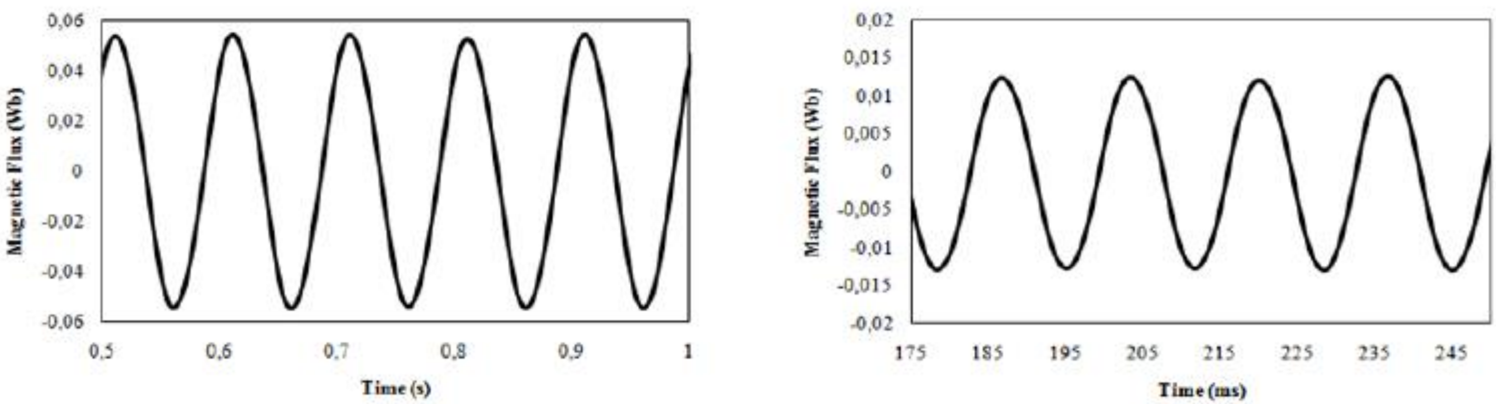

(a) (b)

Temporal magnetic flux ϕ variation: **a)** for ω=100 rpm and **b)** ω=600 rpm.

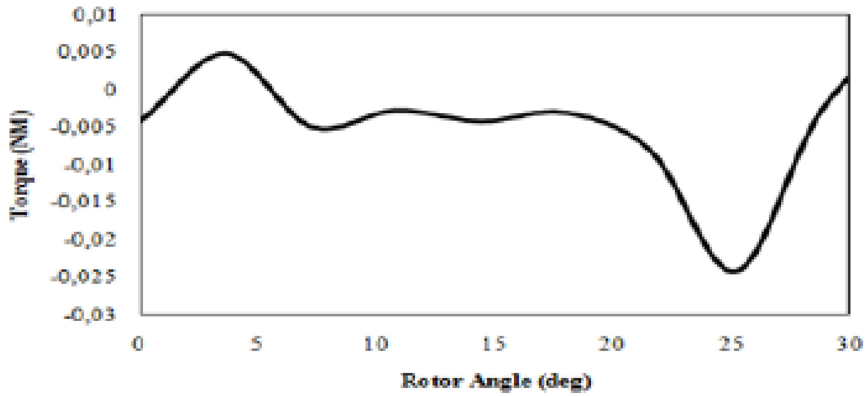

(a)

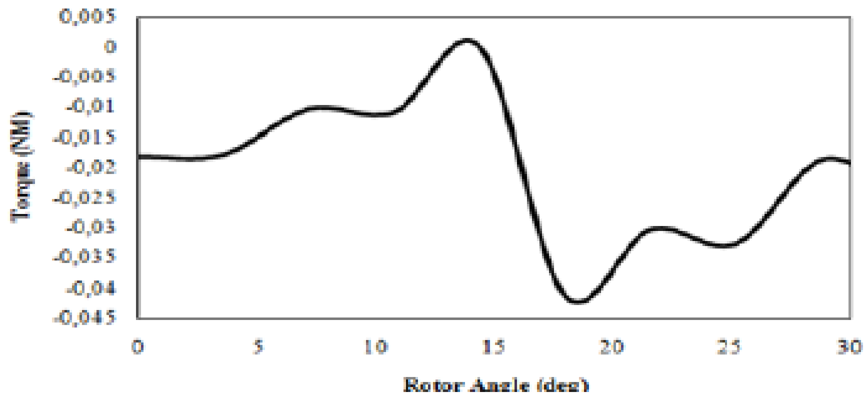

(c)

The cogging torques ω=100 rpm and ω=500 rpm.

The minimal and maximal cogging torque difference is 32 mNm.

Experimental results

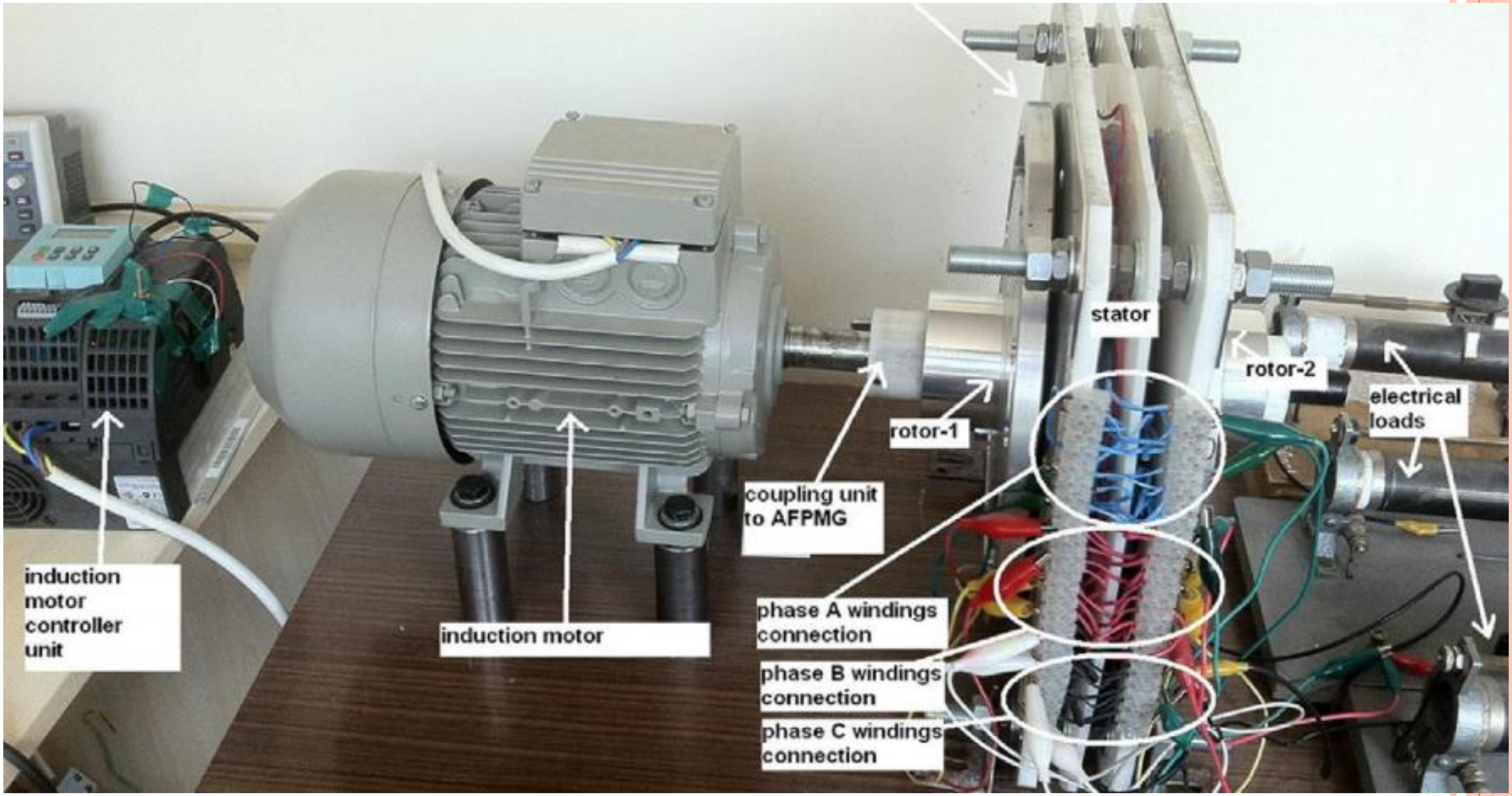

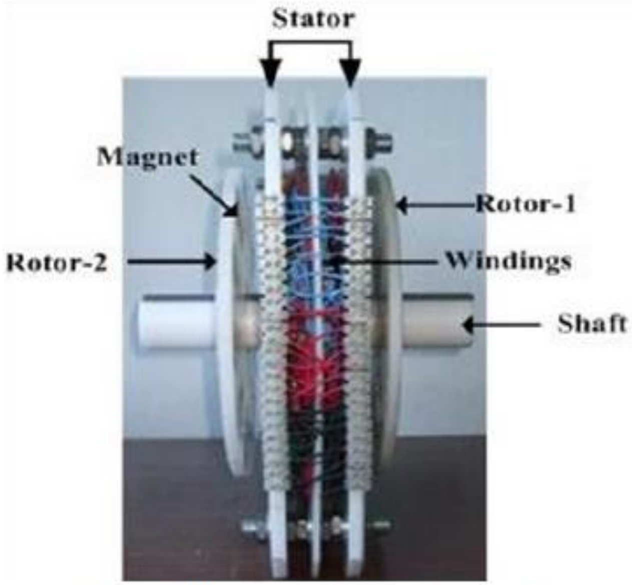

Fig. 16. The single phase generator with radial and axial fluxes. Each coil groupings are denoted by different color.

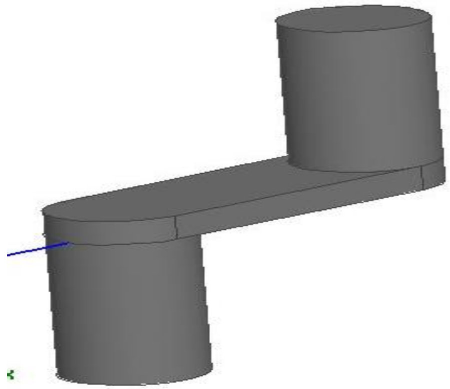

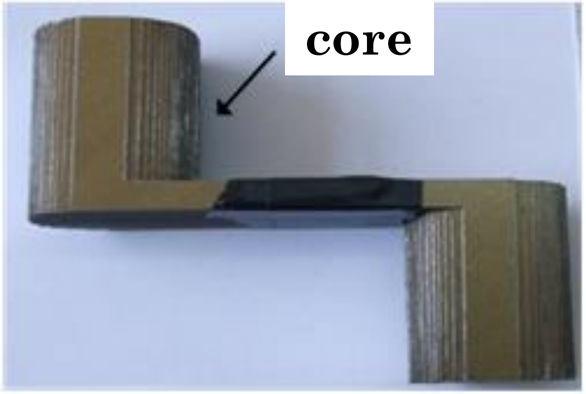

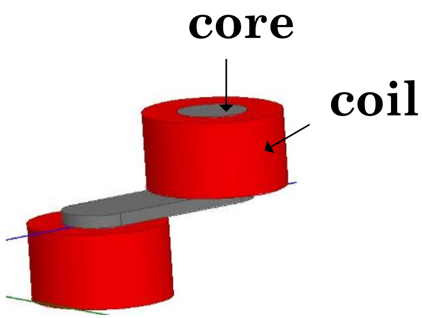

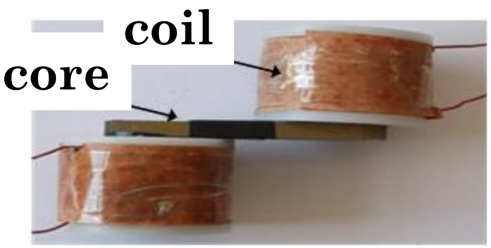

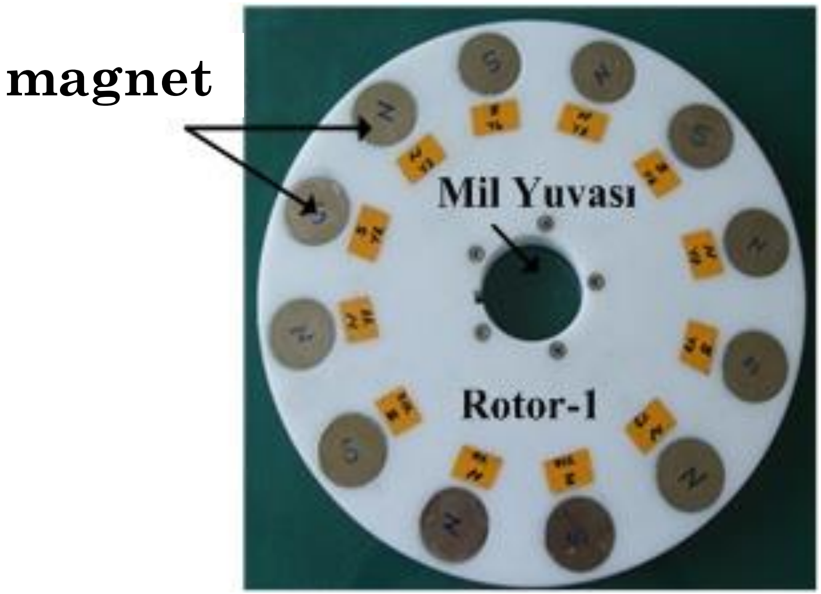
magnet
Mil Yuvası
Rotor-1
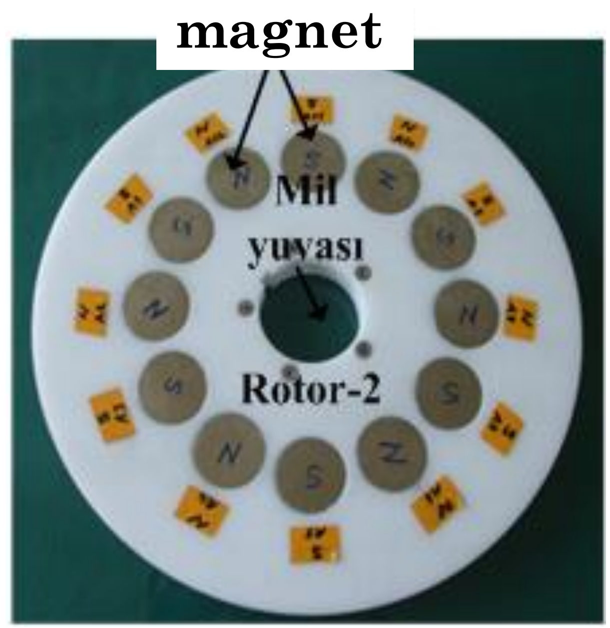
magnet
Mil
yuvası
Rotor-2

Voltage outputs of Gen2

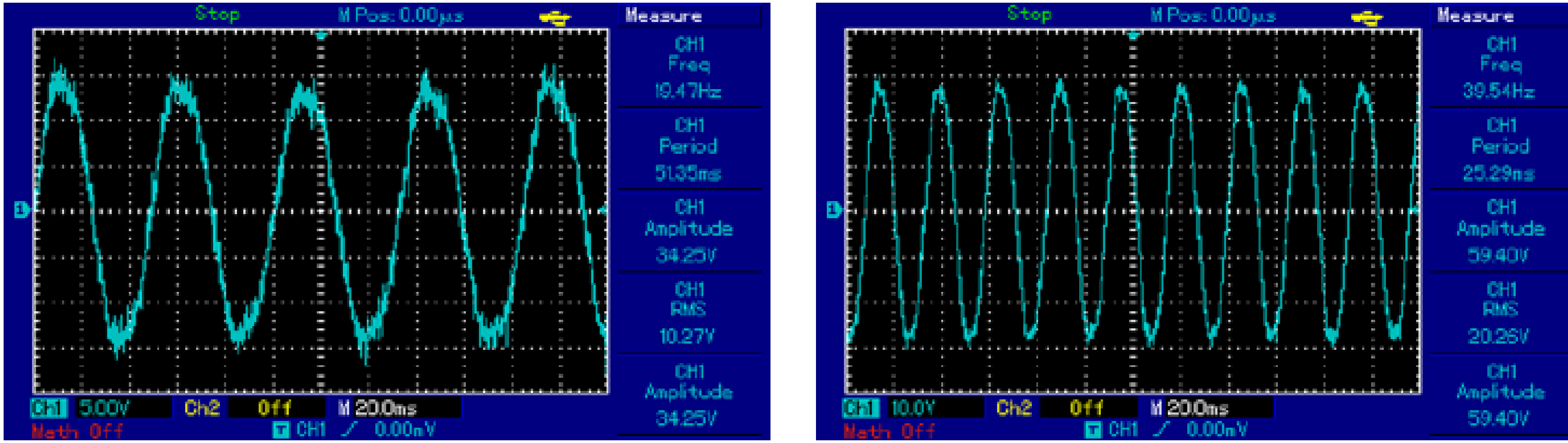

(a) (b)

Fig. 17. No-load voltage outputs of Group A windings. The top and bottom waveforms were taken at 200rpm (a) and 400 rpm (b).

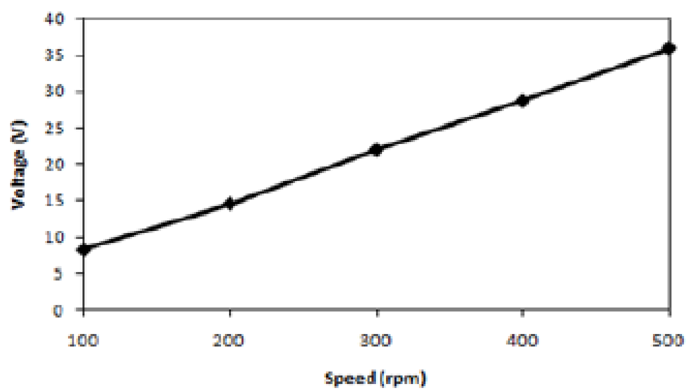

Fig. 18. The generated voltage U_{max} of Group A windings versus rotor speed.

Results from 3-phase machine

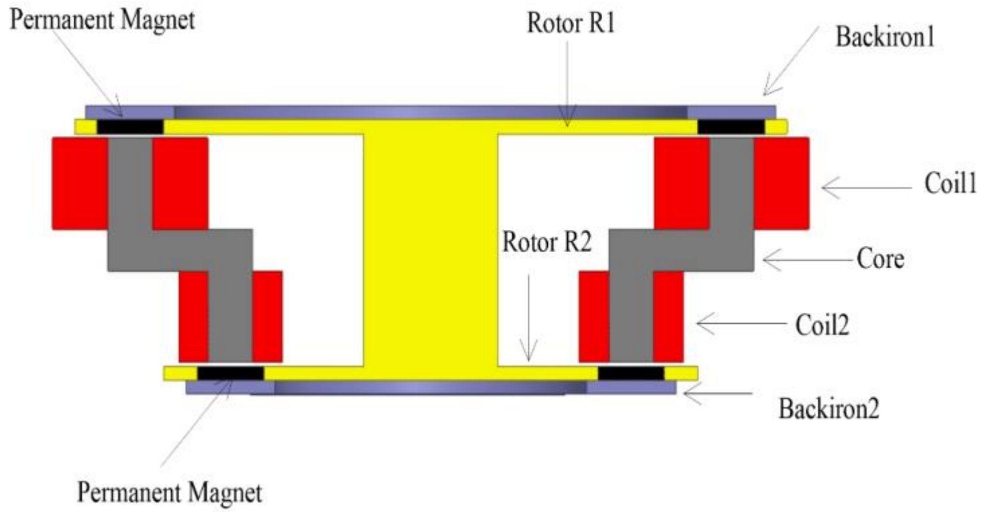

IESRES EU- ERASMUS+
ekurt@gazi.edu.tr

The air gap is adjusted as 1.5 mm for two sides of the stator located at the middle. The cross-section view of the PMG is shown in Fig. 1 . Two rotors are positioned on the upper and lower sides of a stator as seen in Fig. 1. Rotor-1 which has larger coils is located top, whereas the Rotor-2 is located bottom. The cores and the location of sample magnets are also obvious in Fig. 1.

Table 1 – Design parameters of the machine.

Components	Features
Inner radius of rotor R_2 (mm)	75
Outer radius of rotor R_2 (mm)	105
Inner radius of rotor R_1 (mm)	120
Outer radius of rotor R_1(mm)	150
Inner radius of stator disc (mm)	70
Outer radius of stator disc (mm)	155
Thickness of *back-irons* (mm)	5
Radial width of *back-irons* (mm)	40
Coil inner diameter (mm)	30
Small coil outer diameter (mm)	46.4
Large coil outer diameter (mm)	69.6
Phase	3
Winding turns for large coil	300
Winding turns for small coil	200
Coil number	24
Wire diameter (mm)	0.75
Magnet type	NdFeB
Magnet shape	Circular
Magnet number	16
Magnet diameter (mm)	30
Magnet thickness (mm)	5
Core material	M19
Core type	Axially/radially laminated
Core number	12
Air gap (mm)	1.5

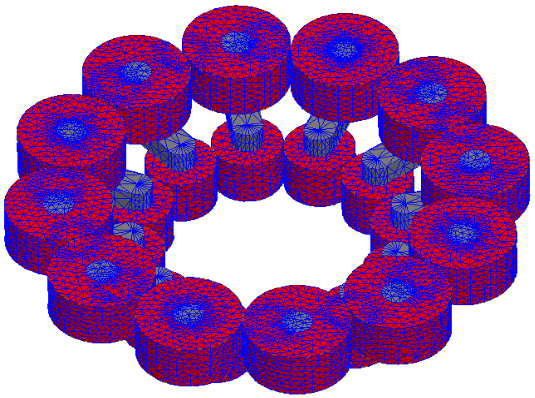

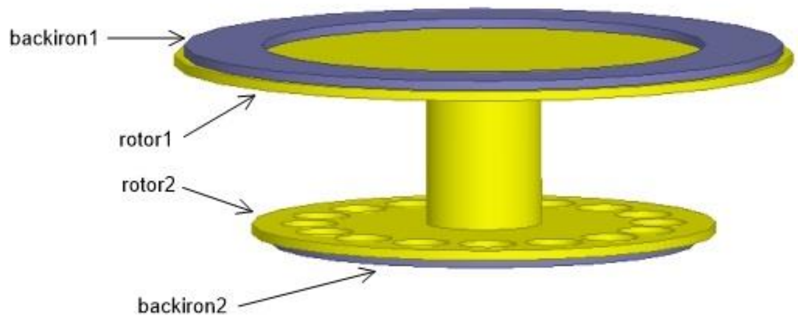

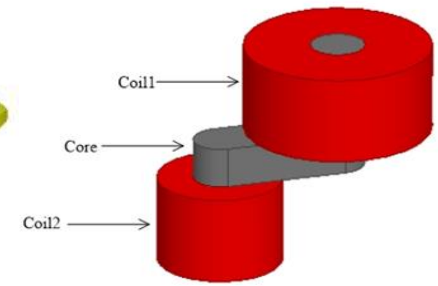

For the electrical connection of the windings, the windings at the top and bottom tips of each core have been connected in series. The adjacent core tips and coils are situated on the stator with an electrical angle of 22.5 degrees. In the rotor unit shown in Fig. 4(b), the magnet housings are indicated on the yellow filling material. There exist 16 circular pair poles in the machine. Note that there exist also housings at the top rotor for the same magnet sizes. The magnets are adjusted as 30 mm in diameter and 5 mm in thickness in the design. In order to sustain maximal flux, the backirons contacts the magnets at both sides.

Magnetostatic Simulations of PMG

From top to bottom, Fig. 5(a) gives the minimal and maximal flux densities of 0.47 T and 1.3 T, respectively. Note that the flux densities become zero at the inner edges of cores. *B* becomes maximal in the core, when two magnets come nearby the core tips as usual. After each 22.5 degrees, four magnets come to the same angular position with the cores. Therefore these regions have the maximal flux on the cores.

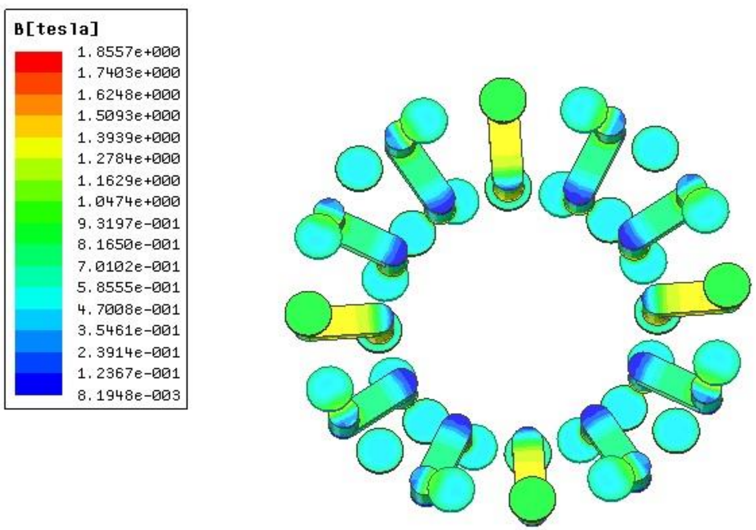

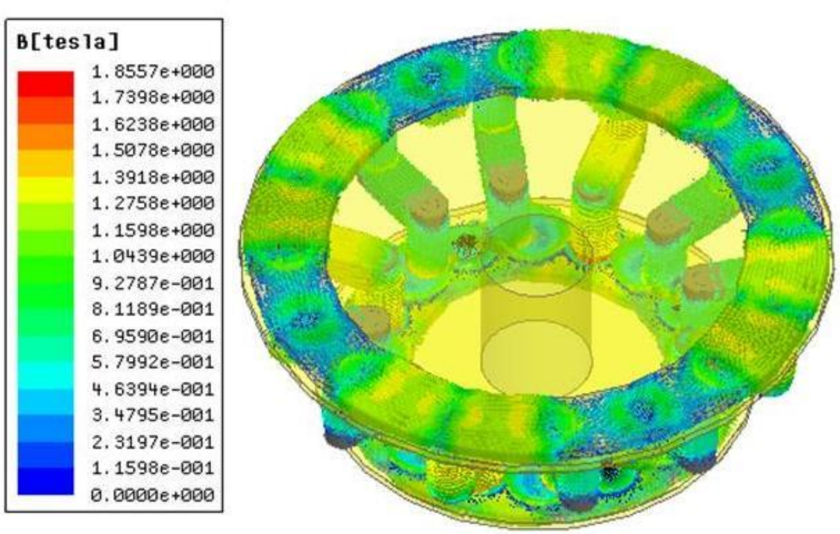

MagnetoDynamics Simulations of PMG

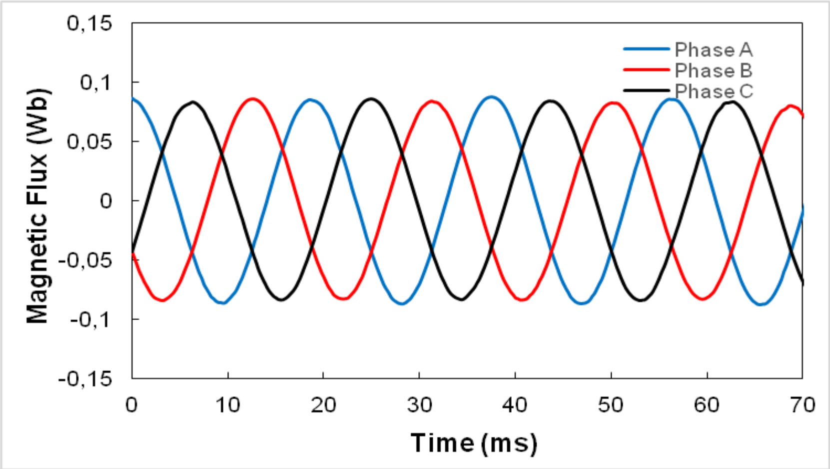

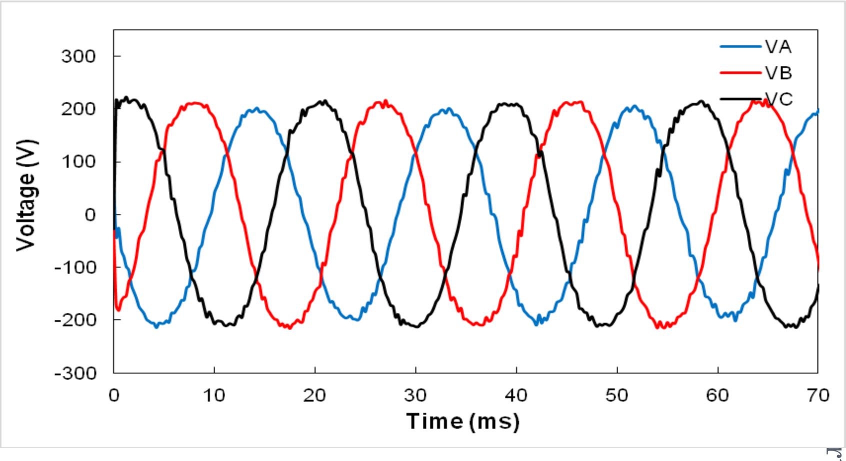

In another recent study of Kurt and Gor [23,24], the maximal magnetic flux of the machine without the backiron has been found as 0.02 Wb at 1000 rpm, whereas in the recent machine 0.08 Wb has already obtained at a lower speed (i.e. 800 rpm). Thus it is proven that the backiron unit in the rotor is vital to increase the flux of the recent machine. Besides, the otimizationb of the airgap value also assists to achieve that finding. Voltage waveform is shown at the right hand-side in the no-load case. Initially, It is obvious that the phases have correct phase shift with the same sinosoidal waveform. Indeed, the maximal amplitude of each phase is obtained with the phase shift of 120 degrees as usual. There exist slight harmonicity due to the transient numerical analyzes, since the time evaluation has not been kept so short. At the rotor speed 400 rpm, the maximal peak to peak voltage is found as $V_{pp} = 222$V.

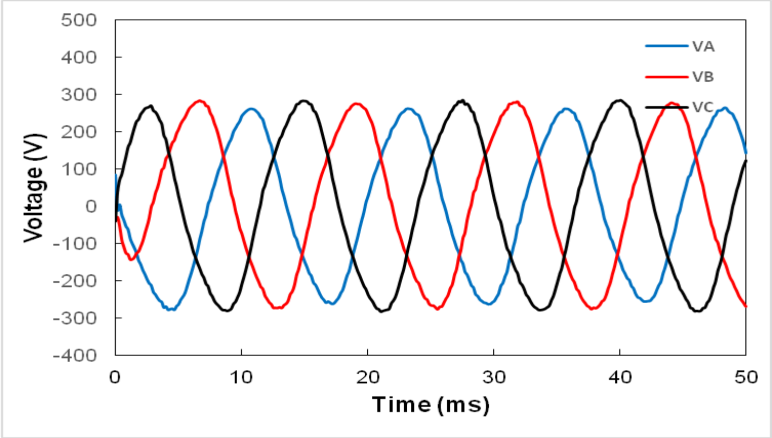

In the case of electrical load (i.e 40 ohms), the maximal voltage value is obtained as 222 V for 600 rpm (see in Fig. 8(a)). It is also interesting that the harmonics decay at in similations with electrical load . In laboratory experiments performed by other machines, these kind of harmonicty annihilations were also observed before after the addiction of the load.

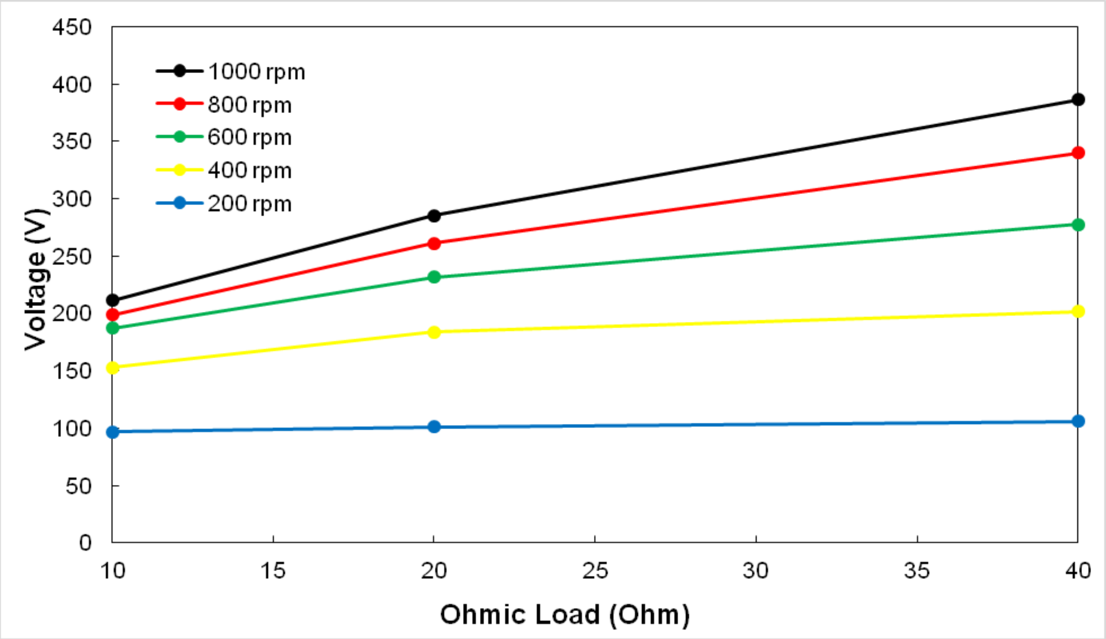

Simulations have been carried out for different electrical loads as seen in Fig. 10. According to the transient simulations, the maximal amplitudes increase upto V= 341 V at the load 50 ohms for 1000 rpm. Indeed, the maximal voltage can be expected for slightly high loads. When the rotor speed increases, linearly the output voltage increases. However, the maximal amplitude becomes 100 V and it does not change for the rotor speed 200 rpm for each loads. While the speed decreases, the increament rate of the amplitude also decreases smoothly as also seen in previous experiments with other generators.

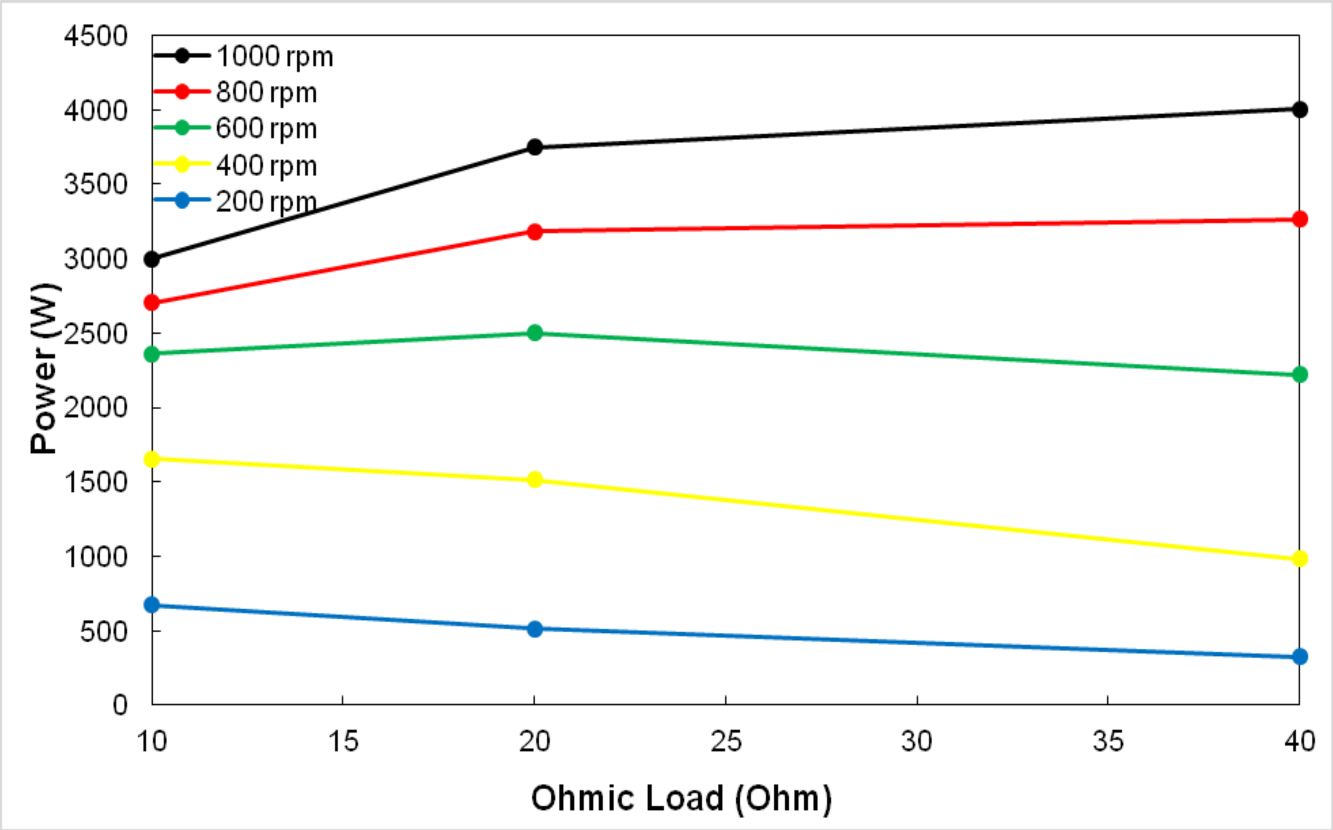

Fig. 11 gives the output power estimation for different ohmic loads in terms of different rotor speeds. Note that it is the power of three phases. While the rated power is obtained around 40 ohms for 1000 rpm, the maximal power gets to lower resistive loads such as 20 ohms and 10 ohms for lower rotor speeds as usual.

The detailed simulations indicate that the power of 4kW is available from the generator at 1000 rpm. The power density of the machine become P_v = 336 kW/m^3, which is a good value for axial generators accroding to the literature if the power densities are considered between 6 kW/m^3 and 700 kW/m^3 [11].

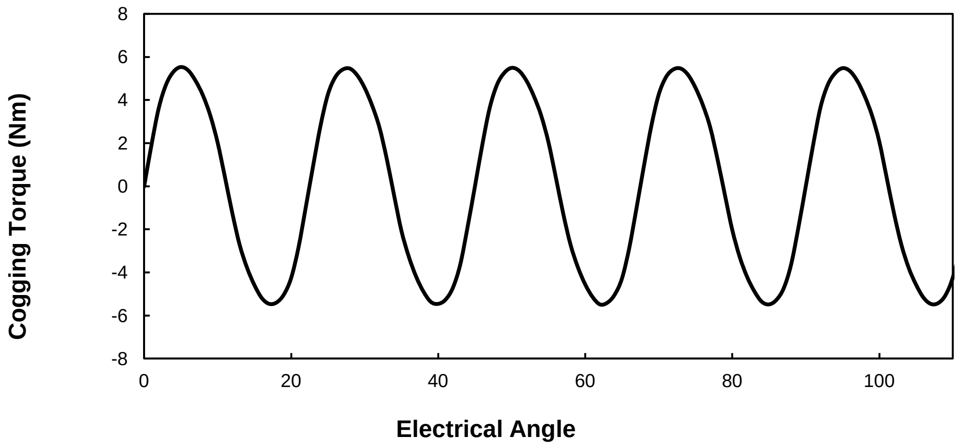

Finally, the result of the cogging torque is given in Fig. 12. The net cogging torque value fluctuates between ± 5.6 Nm. Comparing the previous studies [6,21], it is a good value for an axial generator with cores and back irons. Since the flux increases at the vicinity of core tips, it produces a net torque. Note also that the new shaped core also assists to decrease the torque in that regard.

IESRES EU- ERASMUS+
ekurt@gazi.edu.tr

Table 2 — THD values for various electrical loads at 1000 rpm.

Ohmic load (Ohm)	THD (%)
50	3.4
40	3.4
30	3.2
20	3.1
10	2.9

CONCLUSIONS

- A new axial-field permanent magnet generator (AFPMG) is designed and analyzed electromagnetically.
- This generator has single stator and double rotor.
- This configuration provides a higher magnetic flux density inside the coils and assists to decrease heat produced at high speed continuous operations. The studies on cooling continue.
- The flux lose is minimized by using seperated cores.
- Proposed machine has 24 coils and 32 magnets. But it can be transformed into a single phase phase machine by changing rotors with 12 magnets.

Our Project Web-site: http://ecerg.com/iesres/iesres.html
INNOVATIVE EUROPEN STUDIES ON RENEWABLE ENERGY SYSTEMS (IESRES)

www.ewres.info
4rd European Conference on Renewable Energy Systems (ECRES2016)
ISTANBUL 28-31 August 2016
Receives papers till 15th June 2016.

THANK YOU VERY MUCH

References

[1] G.F. Price, T.D. Batzel, M. Comanescu, B.A. Muller, Design and testing of a permanent magnet axial flux wind power generator, in: 2008 IAJC-IJME International Conference, ISBN 978-1-60643-379-9

[2] A. Aawar, T.M. Hijazi, A.A. Arkadan, Design optimization of axial-flux permanent magnet generator, in: Electromagnetic Field Computation (CEFC), 2010 14th Biennial IEEE Conference, 9-12 May 2010, 10.1109/CEFC.2010.548 1641

[3] G. Duan, H. Wang, H. Guo, G. Gu, Direct drive permanent magnet wind generator design and electromagnetic field finite element analysis, IEEE Transactions on Applied Superconductivity, vol. 20, No. 3, June 2010, pp. 1883-1887.

[4] B. Singh, B.P. Singh, S. Dwivedi, A state of art on different configurations of permanent magnet brushless machines, IE (I) Journal – EL, vol. 78, pp. 63-73, June 2006.

[5] M. Sadeghierad, A. Darabi, H. Lesani, H. Monsef, Design analysis of high-speed axial-flux generator, American J. of Engineering and Applied Sciences 1 (4): 312-317, ISSN 1941-7020,2008.

[6] VV Parlikar, PM Kurulkar, KP Rathod, P. Kumari, An Axial-Flux Permanent Magnet (AFPM) Generator for defence applications - paradigm shift in electrical machine, ACEEE Int. J. on Electrical and Power Engineering, Vol. 03, No. 01, February 2012.

[7] A.P. Ferreira, A.M. Silva, A.F. Costa, Prototype of an axial flux permanent magnet generator for wind energy systems applications, in: Power Electronics and Applications, 2007 European Conference, 2-5 Sept. 2007, Conference Publications, IEEE.

[8] T.M. Jahns, W.L. Soong, Pulsating torque minimisation techniques for permanent magnet AC motor drives: a review, IEEE Transactions on. Industrial Electronics, vol. 43, no.2, pp.321-330. 1996.

[9] D.C. Hanselman, Effect of skew, pole count and slot count on brushless motor radial force, cogging torque and back emf, IEE Proc. Electric Power Applications, vol. 144, no.5, pp. 325-330, 1997.

[10] M.S. Islam, S. Mir, T. Sebastian, Issues in reducing the cogging torque of mass-produced permanent-magnet brushless DC motor, IEEE Transactions on Industry Applications, vol. 40, no. 3, pp 813-820, 2004.

[11] M. Aydin, Magnet skew in cogging torque minimization of axial gap permanent magnet motors, Proceedings of the 2008 International Conference on Electrical Machines, Paper ID 1186, 978-1-4244-1736-0/08/$25.00 ©2008 IEEE

[12] S.P. Barave, B.H. Chowdhury, Optimal design of induction generators for space applications, IEEE Transactions on Aerospace and Electronic Systems vol. 45, no. 3 july 2009.

[13] B. Singh, Recent advantages in permanent magnet brushless DC motors, Sadhana, vol. 22(6), pp. 837-853, December 1997.

[14] J.R. Bumby, R. Martin, Axial-flux permanent-magnet air-cored generator for small-scale wind turbines, Proceedings. IEE- Electrical Power Applications, vol. 152(5), pp. 1065-1075, September 2005.

[15] E. Kurt, S. Aslan, M. Demirtaş, M.E Güven, Design and analysis of an axial-field permanent magnet generator with multiple stators and rotors, Proceedings of the 2011 3. Int. Conf. Power Engineering, Energy and Electrical Drives, Torremolinos (Málaga), Spain. May 2011, 978-1-4244-9843-7/11/$26.00 ©2011 IEEE

[16] http://www.finite-element-method.info

[17] http://www.eng.fsu.edu/~chandra/courses/eml4536/

[18] http://urbana.mie.uc.edu/yliu/FEM-525/FEM_Lecture_Notes_Liu_UC.pdf

[19] E. Kurt, H. Gör, U. Döner, Electromagnetic design of a new axial and radial flux generator with the rotor back-irons, Int. J. Hydrogen Energy, *to be published*.

[20] E. Kurt, H. Gör, Waveform characteristics and losses of a new double sided axial and radial flux generator, *to be published*.